TOPICAL REVIEW

A review of wireless power transfer using magnetoelectric structures

To cite this article: Orpita Saha *et al* 2022 *Smart Mater. Struct.* **31** 113001

IOP Publishing Smart Materials and Structures
Smart Mater. Struct. **31** (2022) 113001 (22pp) https://doi.org/10.1088/1361-665X/ac9166

Topical Review

A review of wireless power transfer using magnetoelectric structures

Orpita Saha[1], **Binh Duc Truong**[2] and **Shad Roundy**[2,*]

[1] Department of Electrical and Computer Engineering, University of Utah, Salt Lake City, UT, United States of America
[2] Department of Mechanical Engineering, University of Utah, Salt Lake City, UT, United States of America

E-mail: shad.roundy@utah.edu

Received 3 August 2022
Accepted for publication 12 September 2022
Published 28 September 2022

Abstract

Wireless power transfer (WPT) has received increasing attention primarily as a means of recharging batteries in the last few decades. More recently, magnetoelectric (ME) structures have been investigated as alternative receiving antennas in WPT systems. ME structures can be particularly useful for small scale devices since their optimal size is much smaller than traditional receiving coils for a given operating frequency. WPT systems using ME laminate receivers have been shown to be helpful in wirelessly powering various sensors and biomedical implants. In recent years, a large number of studies have been conducted to improve the performance of ME composites, in which various configurations have been proposed, along with the use of different magnetostrictive and piezoelectric materials. In addition, many efforts have been devoted to miniaturizing ME devices. An essential obstacle to overcome is to eliminate the need for a DC bias field that is commonly required for the operation of ME structures. In this review paper, we will discuss the basic principle of ME effects in composites, materials currently in use, various ME receiver structures, performance measures, limitations, challenges, and future perspectives for the field of WPT. Furthermore, we propose a power figure of merit which we use to compare recent ME WPT research papers.

Keywords: magnetoelectric effect, magnetostrictive/piezoelectric composites, wireless power transfer, biomedical implants

(Some figures may appear in colour only in the online journal)

1. Introduction

Wireless power transfer (WPT) has become a significant research topic over the past decade owing to its extensive application in powering or recharging wireless devices. Lately, WPT has increasingly been used for biomedical implants where it is used to transmit energy from an external source outside of the body to an implant inside the body [1]. Researchers have taken three main approaches for biomedical WPT: radio frequency (RF) power transfer, acoustic power transfer, and inductive power transfer (IPT). In RF WPT, power can be transferred using a set of transmitting and receiving antennas operating in far-field ranges [2]. Although RF WPT has been convincingly used for biomedical implants [3, 4], there are safety concerns at high power densities resulting from tissue heating. At the high frequencies at which RF WPT operates, energy absorption in human tissue is high, which both reduces

* Author to whom any correspondence should be addressed.

efficiency and results in tissue heating [5, 6]. Acoustic WPT systems transfer power by propagating energy as sound or vibration waves. The propagating energy is collected by a receiver which converts the vibration energy to useful electrical energy [7]. Acoustic WPT works well through soft tissue in systems where the acoustic power transmitter can be in intimate contact with the skin. However, it suffers from a large amount of energy reflection when passing from air to soft tissue and from soft tissue to bone [8]. IPT is the most common method of high power WPT. Power can be transferred over short distances (near-field transfer) by means of inductively coupled coils. However, for very small implants, IPT becomes very inefficient because the small receiving coil size drives up the optimal operating frequency with the attendant higher energy absorption in tissue. This frequency-size tradeoff has led researchers to investigate alternative materials and structures for WPT using magnetic fields. Magnetoelectric (ME) devices convert an applied magnetic field to a generated electric field through strain-mediated coupling. As the resonance frequency of ME structures is a function of the mechanical (or acoustic) oscillation, for a given size, the optimal operating frequency for ME antennas is much lower than for an inductive coil receiver. Thus, there exists the potential for significantly higher power densities at the ME receiver, especially for small devices. Typical ME WPT systems consist of a transmitting coil and a ME receiver [9]. The goal of this paper is to review the use of ME structures as receivers in WPT systems. For a more general review of ME structures and applications, we refer the reader to Palneedi *et al* [10]. In this article, we will restrict ourselves specifically to the application of WPT.

ME materials couple the magnetic and electric properties of the material. Although single phase ME materials exist [11], the best performance has been achieved using composites of magnetostrictive (MS) and piezoelectric materials [10]. Field-induced magnetostriction occurs when strain is induced in a ferromagnetic (FM) material by an applied magnetic field [12]. Magnetostriction appears as a result of magnetic domains (which may be randomly aligned) aligning with the applied magnetic field and domain walls shifting [13]. The MS coefficient (λ) is defined as the strain resulting from the applied magnetic field:

$$\lambda = dl/l \tag{1}$$

where l is the specimen length.

Figure 1 shows a typical curve of the MS coefficient as a function of applied magnetic field. Once the magnetic domains are fully aligned with the applied field, the MS coefficient saturates at a value of λ_s. Most FM materials are weakly magnetostrictive, however some alloys can exhibit a much larger MS coefficient (see section 2). (Note, some authors use the term 'magnetostriction' to refer to the saturation value of the MS coefficient, λ_S, while others use the term to refer to the MS coefficient, λ. We will use 'magnetostrictive coefficient' to refer to λ and 'saturation magnetostriction' to refer to λ_S.)

A ME composite couples the magnetic and electric properties of the constituent materials. This process is illustrated

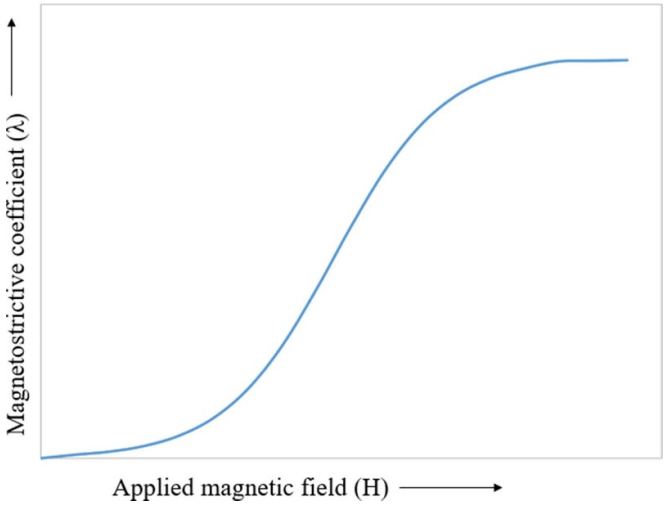

Figure 1. MS coefficient vs applied magnetic field.

in figure 2. The MS phase develops a strain in response to an applied magnetic field (H) as a result of the MS effect. This strain is mechanically transferred to the piezoelectric material through an interface layer, which then produces a transverse dielectric polarization through the 3–1 mode piezoelectric effect [14]. Although the ME effect exists in some single-phase materials (i.e. CO_2O_3), it is more than two orders of magnitude larger in composites than in single-phase materials [15].

In section 2 of this paper, we discuss materials used for ME composites along with the important material parameters for ME WPT. We explain different ME structures that are utilized in the field of WPT in section 3. Many ME transducers require a DC magnetic field bias for their operation (see section 4), which can limit possible applications. Therefore, we next discuss approaches to overcome the need for an external magnetic field bias (i.e. self-biasing approaches) in section 5. We also develop a power figure of merit (FOM_P) for ME WPT receivers and compare devices from the literature using this figure of merit in section 6. Finally, we identify some specific areas in which more research is needed to improve the performance of ME structures in section 7.

2. Materials

ME materials exhibit magnetic field induced electrical polarization and electric field induced magnetization. ME devices can be made in single-phase, particulate composites, thin-film based composites, or bulk material laminated composites [16]. At room temperature, most single-phase materials have either low permittivity or low permeability and thus exhibit poor ME coupling. The archetype of single-phase ME compounds, $BiFeO_3$ for instance, shows strong ferroelectricity but poor FM properties above room temperature [10].

ME composites are made of combinations of highly MS materials and piezoelectric materials. The strength of the ME coupling in the composites depends on the properties

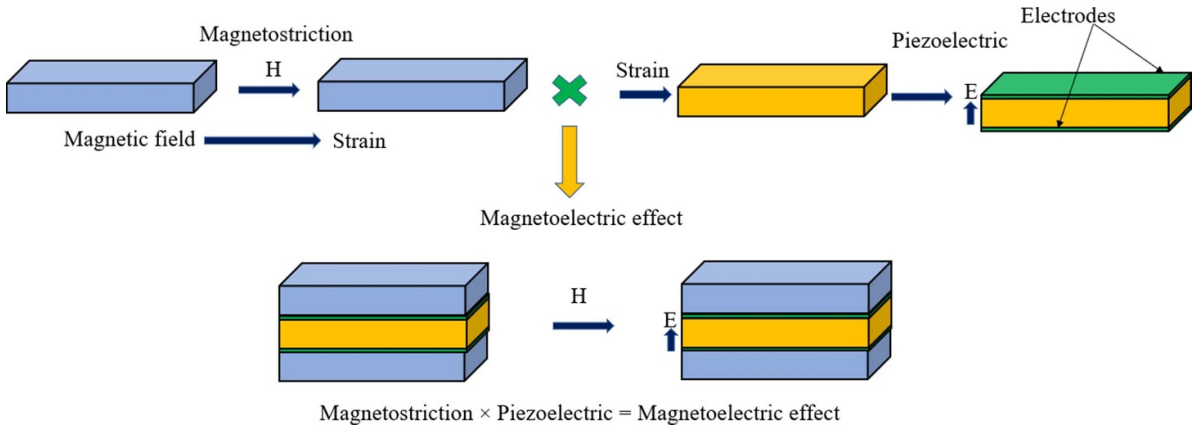

Figure 2. Schematic illustration of strain-mediated ME effect in a composite system consisting of a magnetic layer (blue) and a piezoelectric layer (yellow). Reproduced from [14], with permission from Springer Nature.

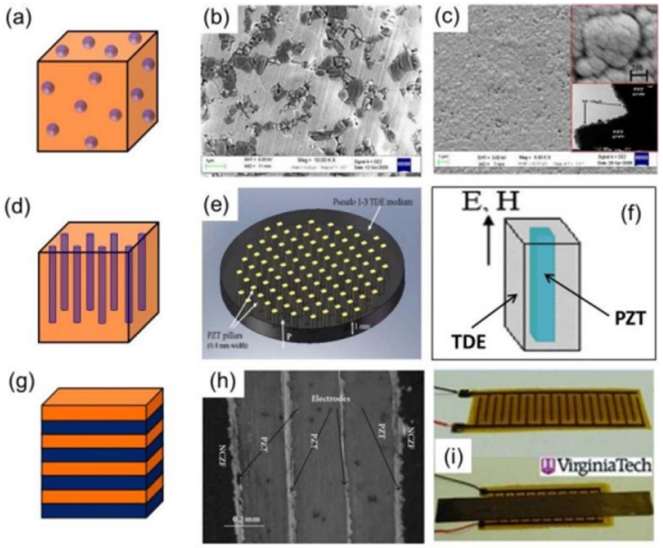

Figure 3. Phase connectivity of ME composites. (a)–(c) A 0–3 connectivity, (d)–(f) 1–3 connectivity, (g)–(i) 2–2 connectivity. Reproduced from [10]. CC BY 4.0.

of both the piezoelectric and MS materials, the manufacturing process, the interfacial coupling, and the phase connectivity (i.e. the connectivity of the magnetic-piezoelectric phases described by 0–3, 1–3, and 2–2, respectively). Referring to figure 3, in the 0–3 particle-matrix composites, magnetic particles are embedded in the piezoelectric matrix. A 1–3 cylinder-matrix composites are formed by embedding magnetic fibers/rods/tubes/wires in the piezoelectric matrix. The particles (in the 0–3 composite) and fibers (in the 1–3 composite) can be either randomly dispersed or periodically aligned. A 2–2 laminate composite consists of alternating magnetic and piezoelectric layers. Such laminates can be fabricated in different shapes and geometries, including discs, squares, rectangles, and rings, with various dimensions. They can be arranged as bilayered and multilayered structures [10].

Several ME composites have attracted extensive attention in recent years. Since the introduction of the 2–2 layered structure by Ryu *et al* [17], significant progress has been made. Findings have shown that the 2–2 laminate bimorph composites have a higher ME response and are comparatively simpler to manufacture than 0–3 or 1–3 composites [18]. Moreover, because the piezoelectric and magnetic phases are spatially isolated, these composites can be electrically and/or magnetically poled to a higher degree, thus providing higher ME coupling within the layered composite system [19]. In this article, we describe mostly 2–2 composite laminated ME devices for converting wirelessly transmitted magnetic energy due to their higher performance and relative maturity [10].

Truong and Roundy developed an analytical model to describe WPT to a ME 2–2 laminate [8]. A 2–2 laminate can operate in four different modes: longitudinally magnetized and longitudinally poled (L–L), transversely magnetized and transversely poled (T–T), transversely magnetized and longitudinally poled (T–L), longitudinally magnetized and transversely poled (L–T) [20]. These modes are depicted in figure 4 along with standard axis definitions. The L–T mode is the most common due to the combination of high magnetic-electrical coupling and ease of manufacture, and the mode analyzed by Truong and Roundy. However, the general insights from their model are broadly applicable to any of the four configurations.

The experimentally validated model from Truong and Roundy identifies two key material parameters that govern the electrical power generation of the ME laminate receiver: the electromechanical transduction factor (Γ_p) for the piezoelectric layer, and the magneto-elastic transduction factor (Γ_m) for the MS layer(s):

$$\Gamma_p = -w\frac{d_{31,p}}{s_{11}^E} \tag{2}$$

$$\Gamma_m = 2wt_m\frac{d_{33,m}}{s_{33}^H} \tag{3}$$

where s_{11}^E and s_{33}^H are the elastic compliance of the piezoelectric layer at constant electric field and the elastic compliance of the MS layer(s) at constant magnetic field, w is the width of laminate (assumed to be the same for all layers), t_m is the thickness of a MS layer, $d_{31,p}$ is the transverse piezoelectric strain

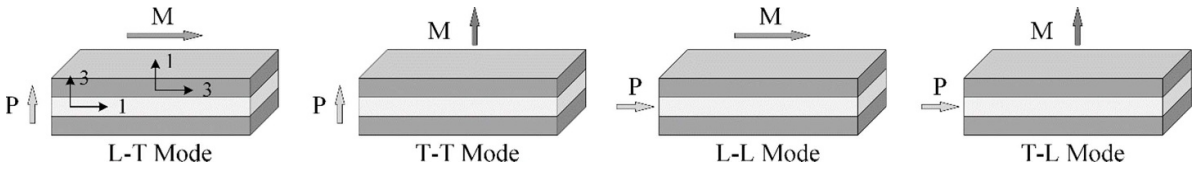

Figure 4. Four 2–2 composite laminate configurations. Dark gray indicates MS material, light gray indicates piezoelectric material. Coordinate frames indicated for MS and piezoelectric materials for the L–T mode.

Table 1. Common MS materials and alloys and relevant material constants.

MS materials	μ_r	s_{33}^H, $m^2\,N^{-1}$	$d_{33,m}$, $m\,A^{-1}$	FOM_{MS}, $N\,A^{-1}m^{-1}$	References
Nickel	100–600	4.9×10^{-12}	1.25×10^{-9}	255	[16]
Terfenol-D	6	40×10^{-12}	1.2×10^{-8}	300	[23]
Galfenol	100	2.5×10^{-11}	7.77×10^{-9}	311	[8]
Metglas	40 000	40×10^{-12}	5.03×10^{-8}	1258	[16]

Note: $d_{33,m}$ values are all non-resonant.

Table 2. Common piezoelectric materials and relevant material constants.

Piezoelectric materials	$\varepsilon_{33}^T/\varepsilon_0$	s_{11}^E, $m^2\,N^{-1}$	$d_{31,p}$, $pC\,N^{-1}$	FOM_{PE}, $C\,m^{-2}$	References
PZT 5	2300	14.8×10^{-12}	−310	−20.9	[23]
PZT 4	1350	12.2×10^{-12}	−123	−10.1	[16]
PMN–PT	2134	69×10^{-12}	−1330	−16.4	[23]
AlN	10.5	2.85×10^{-12}	−1.73	−0.61	[16]
PVDF	8–10	1.75×10^{-10}	22	0.125	[24]

constant, and $d_{33,m}$ is the longitudinal piezomagnetic constant. For a further description of the material orientations and resulting subscripts in these equations we refer the reader to [8].

Neglecting the geometric terms in equations (2) and (3) in order to focus on material properties, the important piezoelectric material figure of merit is $d_{31,p}/s_{11}^E$. The piezoelectric d coefficient is the ratio of the mechanical strain developed in response to an applied electric field. Common piezoelectric materials with high d coefficients are shown in table 1. The ideal piezoelectric material has a high d coefficient and is stiff (i.e. low s_{11}^E). As in the case of the piezoelectric material, the ideal MS material is also stiff (i.e. low s_{33}^H). The piezomagnetic constant $d_{33,m}$ is determined by the slope of the magnetostriction curve ($d\lambda/dH_{DC}$) [21] (see figure 1). It represents the change in strain due to the change in applied magnetic field. As is clear in figure 1, $d_{33,m}$ is strongly dependent on the bias level of the magnetic field. Highly MS materials are generally alloys of rare earth metals with transition metals [12].

Various studies have utilized the ME coefficient ($\alpha_{ME} = V/(t_p H_{ac})$) as a figure of merit for ME structures. Here, H_{ac} is an AC applied magnetic field usually superimposed on a DC bias field to achieve a high piezomagnetic constant. The ME coefficient is also dependent on $d_{31,p}$ and $d_{33,m}$ [21]. However, maximizing α_{ME} is not always equivalent to maximizing the power generation capability of the piezoelectric laminate. For a more in-depth treatment of the relationship between the ME coefficient power conversion, we refer the reader to [8]. For the purposes of this paper we focus on the electromechanical (Γ_p) and magneto-elastic (Γ_m) transduction factors which relate more directly to power generation capability.

Tables 1 and 2 show several common MS and piezoelectric materials along with relevant material properties. Relative magnetic permeability, μ_r, (for MS materials) and relative electrical permittivity at constant stress, $\varepsilon_{33}^T/\varepsilon_0$, (for piezoelectric materials) are shown in addition to the mechanical compliance, d constants, and material figures of merit (FOM_{MS} and FOM_{PE} for MS and piezoelectric materials respectively). Commonly used MS materials for laminated composites include Terfenol-D ($Tb_xDy_{1-x}Fe_2$), Galfenol (FeGa), nickel (Ni), Metglas (FeSiB). (Note, Metglas is a common trade name for a range FeSiB alloys, only some of which exhibit strong magnetostriction.) Samfenol ($SmFe_2$) and FeNi alloy have also been used [22], however, complete material properties are not available in the literature. Commonly used high performance (i.e. high $d_{31,p}/s_{11}^E$) piezoelectric materials include various formulations of lead zirconate titanate PZT ($Pb[Zr_xTi_{1-x}]O_3$), and single crystal PMN–PT ($Pb(Mg_{1/3}Nb_{2/3})O_3$–$PbTiO_3$). We also include aluminum nitride (AlN) which has become more common as a thin film piezoelectric transducer material. Finally, we include polyvinylidene fluoride (PVDF) ($-(C_2H_2F_2)_n-$), a piezoelectric polymer, due to its high mechanical toughness and low cost. The material properties shown are those that are especially relevant for a 2–2 laminate in the L–T mode. We have focused on bulk materials rather than thin films with the exception of AlN. Tables 1 and 2 should not be seen as comprehensive in any way, and are only intended to provide a small sampling of the most commonly used materials for ME WPT. Comparing the material figures of merit, one can quickly see that Metglas and PZT or PMN–PT would provide the highest

material figures of merit. We note that a significant range of material properties exists for various formulations of PZT and those shown in table 2 are just two examples. As a final note, Terfenol-D and Galfenol have higher saturation magnetostriction than Metglas, but lower piezomagnetic constants which is the important parameter for both WPT and a high ME coefficient.

3. Device approaches

Researchers have taken various structural approaches to develop ME devices for WPT. These attempts can be categorized into three main categories as follows: (a) bending structures with masses (sometimes magnetic) placed on a tip of a ME laminated composite cantilever beam, here referred to as the ME–MME configuration. (MME is an acronym for mechano-magneto-electric [8]). (b) ME resonators operating in the longitudinal mode. And (c), ME bending bimorphs composed of one MS layer and one piezoelectric layer. All ME structures under investigation are variants of the 2–2 composite presented in the previous sections. We note that MME devices formed by permanent magnet masses mounted on a piezoelectric beam tip whose substructure is not MS material, e.g. [25], are not considered in this review.

3.1. ME–MME configuration

ME–MME structures are defined by the following key feature, a mass placed at the end of a bending ME structure. This mass is often made of hard magnetic material (i.e. a permanent magnet) that is not highly magnetostrictive itself. The magnetic mass can serve three roles, sometimes simultaneously: it lowers the resonance frequency of the structure, it can directly interact with applied (or ambient) magnetic fields to apply a torque to the end of the structure, and it can apply a DC bias field to the MS material. The application of DC bias fields is the subject of section 4, and will be covered in more detail in that section.

Dong *et al* [26] developed a multimodal system that can scavenge energy from both the magnetic fields and vibration from the environment. The structure consists of a mass at one tip of the beam to lower the resonance frequency. (The authors do not explicitly state whether the mass is magnetic or not, but we believe it is non-magnetic.) The center of the beam comprises a symmetric ME composite (see figure 5). Two PZT fiber layers with push–pull type symmetric polarization units are laminated together with four MS FeBSiC ribbons. A power density of 2.1 mW $Oe^{-1}\,cm^{-3}$ was reported, with a 50 kΩ load under the first longitudinal mode resonance frequency of 21 kHz and an AC magnetic field of 1 Oe, without any mechanical vibration. This experiment was conducted without the tip mass, and the power density was computed based on the laminate volume only. With the presence of the mass, a bending resonance frequency of 40 Hz was observed. A power density of 400 μW $g^{-1}\,cm^3$ was obtained at an optimal load resistance of 3 MΩ and under excitation of 1 g, with no excitation

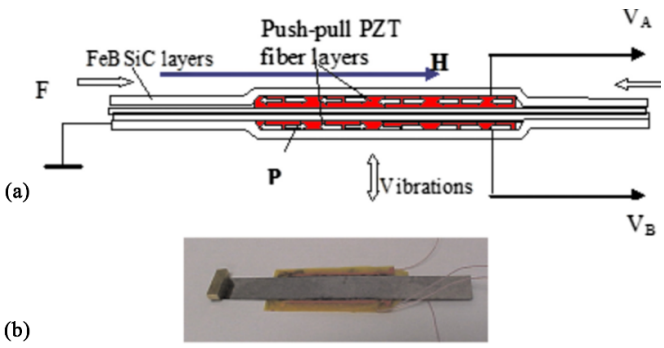

Figure 5. (a) Schematic of ME laminate, and (b) photo of ME laminate. Reprinted from [26], with the permission of AIP Publishing.

from magnetic fields. The system demonstrated the capability to harvest energy from two different sources simultaneously. However, it is not clear how efficient the device was under the combination of the two excitations since no relevant output power or power density was shown.

Gao *et al* [27] fabricated an asymmetrical ME composite Metglas/Pb(Zr,Ti)O_3 operating in bending mode with interdigitated electrodes on the piezoelectric layer. Permanent magnet tip masses were placed on two edges of the composite to decrease the resonance frequency of the laminate and supply the DC bias field for the ME effect. Five Metglas foils of 80 mm in length and 10 mm in width were bonded together, and subsequently laminated to the bottom surface of the PZT fiber layer (40 mm × 10 mm). An output power of 16 μW Oe^{-1} was reported with a 6 MΩ resistance load at 60 Hz resonance frequency.

Ryu *et al* [28] designed a ME–MME generator that can turn on 35 LEDs and drive a wireless sensor network under a magnetic field of 500–700 μT at a low frequency of 60 Hz. This ME–MME resonator is comprised of a ME cantilever beam combined with a neodymium permanent magnet mass, in which the ME laminate was formed by the ⟨011⟩ oriented anisotropic single crystal fiber composite (SFC) piezoelectric layer bonded to a Ni plate. The device operates in bending mode with a resonance frequency around 60 Hz. Including the total volume of the ME laminate and the proof mass, the ME–MME transducer with anisotropic ⟨011⟩ SFC operating in d_{32} mode can provide ∼1600% larger power density (46.3 μW $cm^{-3}\,Oe^{-2}$) than that of the MME generator with isotropic ⟨001⟩–d_{31} mode SFC (2.9 μW $cm^{-3}\,Oe^{-2}$).

Annapureddy *et al* [29] introduced a bending mode cantilever structured ME device with low loss piezoelectric single crystal fiber, Ni sheet and a neodymium permanent magnet proof mass. The hysteresis of the piezoelectric materials, which relates to losses such as dielectric loss (inverse of the electrical quality factor) and mechanical loss (inverse of the mechanical quality factor), causes performance degradation of the device. One method to improve the piezoelectric properties of the PMN–PZT single crystals is to change the dopant (MnO or WO_3) and dopant amount in the composition. A structure with low-loss PMN–PZT single crystal micro fibers was able

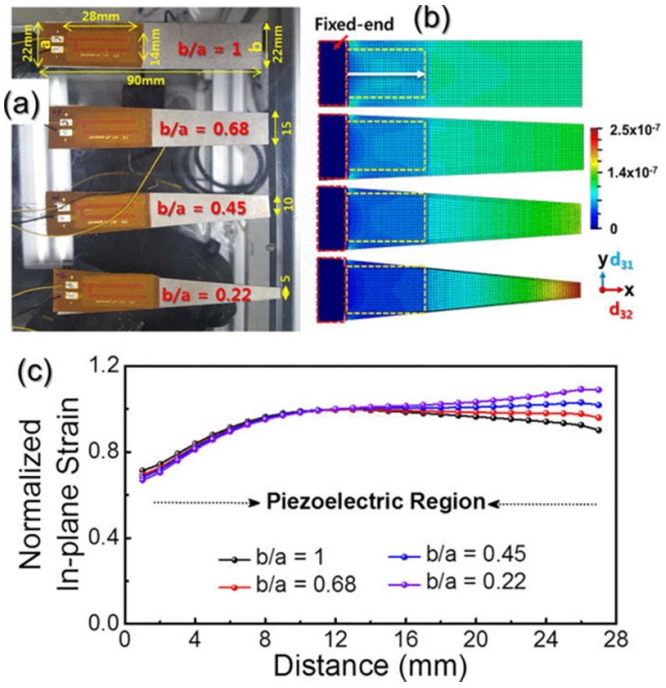

Figure 6. (a) ME structures of various shapes, (b) strain distribution by finite element modeling, and (c) normalized analytical data along the beam central line marked white arrow in (b) in the piezoelectric region. Here, the mid-point of the piezoelectric region is treated as the normalized position for all the structures. The position of an active piezoelectric region was indicated by a yellow-colored dashed rectangle. Reprinted from [30], with the permission of AIP Publishing.

to produce a high open-circuit voltage of 94 V and a short-circuit current of 120 μA, from a magnetic field of 700 μT and at a resonance frequency of 60 Hz. The power density per volume corresponding to the optimum output power was 2.1 mW cm^{-3}. We note that these ME composites, which use Ni as a MS phase, also exhibited self-biased behavior. In particular, the low-loss device attained a ME coefficient of 11.3 V cm^{-1} Oe^{-1} at its bending resonance frequency of 800 Hz, in which neither the magnet mass nor the DC bias field were present.

As a continued work of [29], Annapureddy *et al* [30] further optimized the ME–MME cantilever beam by tailoring the geometry to obtain higher output performance as shown in figure 6. ME composites were clamped at one end, and a magnetic mass of 4.5 g was mounted on other. The shapes and positions of the piezoelectric material and the tip mass were unchanged. But the shape of the beam, as well as the MS Ni layer, was varied. In particular, the free end width of the cantilever changed from a conventional rectangular to a truncated shape, approaching a triangle. A maximum output power density of 27 μW Oe^{-2} cm^{-3} was attained using the tapered-shape ME–MME generator at its resonance frequency of 40 Hz and with an optimal resistive load. The maximum power was improved by 680% with the use of the truncated shape, compared to that of the regular rectangular structure. The authors found that the tapered beam resulted in a higher average in-plane strain energy in the active piezoelectric region than the conventional rectangular or other designed structures. There was an improvement in the vibration displacement of the beam tip, which was possibly due to the decrease of the mechanical damping coefficient. This characteristic could also contribute to the increase in output power.

In 2018, Annapureddy *et al*. [31] designed a ME–MME generator similar to their previous work in [29]. However, the MS material used was Fe–Ga alloy instead of Ni. The ME–MME generator consisted of a cantilever beam with six NdFeB magnets as a proof mass, piezoelectric single crystal macro-fiber composite and a highly textured MS Fe–Ga alloy. Compared to the Ni-based ME–MME generator, a higher power density of 3.22 mW cm^{-3} was obtained under an applied AC field of 7 Oe and at a resonance frequency of 60 Hz. Moreover, a ME coefficient of 26 V cm^{-1} Oe^{-1} was achieved when investigating the Fe–Ga-alloy ME composite alone, without clamping and proof mass. This result was 153% larger than that of the Ni-based structure at its resonance (∼900 Hz). As expected, the piezomagnetic property of Fe–Ga is better than Ni. Based on the frequency response of the output voltage, we observed an increase of the mechanical quality factor, or equivalently, a decrease of the mechanical loss. Therefore, it was not clear whether the improvement of the output power came from the enhancement of the ME effects, or the increase of the mechanical quality factor.

Kang *et al* [32] utilized a ME laminate with MFC (piezoelectric macro fiber composite) and FBS (MS multilayer amorphous $Fe_{85}B_5Si_{10}$) as a cantilever and mounted a magnet mass on its tip to form a ME–MME generator. The magnetic tip mass then, (a) interacts with the external 60 Hz magnetic field to induce vibrations in the beam, (b) applies DC bias field to the FBS layers to maximize the ME coupling, and (c) facilitates the positioning of bending resonance frequency around 60 Hz. FBS alloys were used since they have a high piezomagnetic constant and a low saturation magnetic field. The output power the ME-coupled-MME transducer (MS cantilever beam) is about 1.25 times higher than that of a similar MME device (nonmagnetic beam), 9.73 and 4.32 mW_{peak}, respectively. Correspondingly, the power density was 2.01 mW cm^{-3} when the tip mass volume is included, and 9 mW cm^{-3} when excluding tip mass volume, under an AC field of 10 Oe. The obtained results were better than previous MME generators, such as [29, 30]. Later, Lu *et al* [33] argued that their ME–MME resonator made with PZT and Ni exhibits comparable performance with that in [32]. An advantage of the PZT/Ni configuration is that it is more cost-effective. The acquired output power allowed the energy harvester to turn on 100 commercial LEDs without a power storage unit.

Most ME–MME structures use magnets at the end of the beam, which do not provide a uniform magnetic field inside the material. In order to overcome this limitation, Sriramdas *et al* [34] proposed a concept of distributive forcing by using a dual magnetic mass instead of a single tip mass as shown in figure 7. According to the experimental analysis and simulation results presented, the distributed forcing method led to a 280% improvement in output power in comparison with the

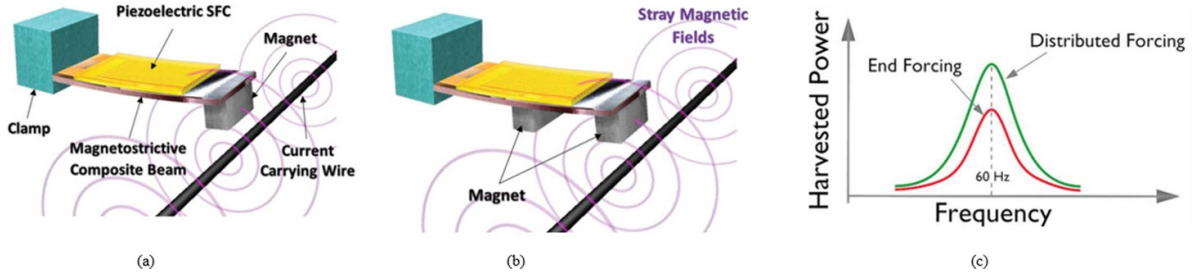

Figure 7. (a) End forcing ME structures, (b) distributed forcing ME structures, and (c) comparison of the normalized power of both structures. [34] John Wiley & Sons. © 2020 WILEY-VCH Verlag GmbH & Co. KGaA, Weinheim.

end mass structure. The ME–MME laminates are composed of one layer of single crystal fiber PMN–PZT and 18 layers of Metglas. The laminate was exposed to a 10 Oe magnetic field at 60 Hz. The authors compared the performance of the two following structures: (a) one magnet placed at the beam tip, and (b) dual-mass configuration, in which one magnet was at the tip and the other magnet was placed 33 mm away from the clamped end. The magnet mass and position play an important role in matching the resonance frequency with the magnetic field frequency in the environment. Therefore, the selection of these two factors is essential, especially in maximizing the power harvested from a power line. The dual mass system produced 2.2 mW cm^{-3}, which is much higher than that of the end mass structure which produced 0.2 mW cm^{-3}.

Lee *et al* [35] proposed a configuration of ME–MME transducer containing multiple layers of Metglas and PZT in order to generate high power output from low input magnetic field, as shown in figure 8. The PZT plates are connected in series and the magnetic tip masses are placed at the end of the beam for magnetizing the Metglas. Since the magneto-mechanical torque (τ) acting on the permanent magnet depends on its magnetization (M) and volume (V), the authors chose a large magnetic tip mass to amplify the torque ($\tau = (M \times B) \cdot V$). Such a ME–MME structure was capable of producing power in the mW range with an input AC magnetic field of 500 μT. For instance, a device with four Metglas layers produced 0.94 mW cm^{-3} under the resonance condition (60 Hz) and a field strength of 300 μT. This prototype led to 300%–400% improvement compared to previously reported ME–MME structures.

An approach that adds a magnetic flux concentrator along with the ME–MME laminates was suggested by Song *et al* [36], which resulted in higher power output compared to conventional ME–MME structures. The ME composite was fabricated with Mn doped piezoelectric single crystal fiber and a truncated shaped nickel cantilever as shown in figure 9. A magnetic mass was mounted at the beam tip. The laminate was placed near a MFC, which is made of nickel layers 0.25 mm thick. The shape and the optimal position of the MFC were determined by COMSOL simulation. The simulated results showed that the MFC was helpful to amplify the flux density. The increased flux density enhanced the magnetic torque applied to the proof mass, which in turn improved the output power. The device with the MFC generated a power density

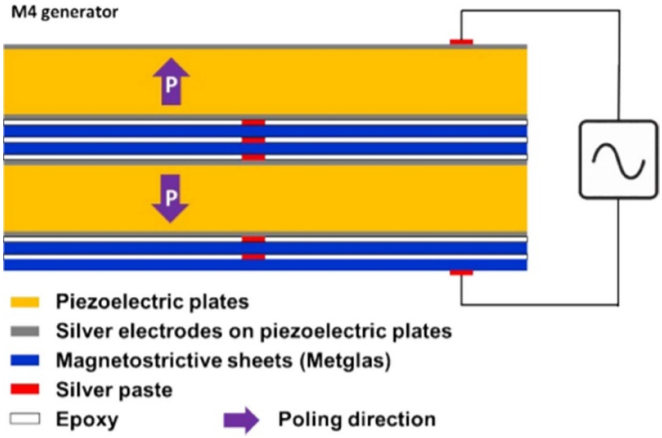

Figure 8. Cross-sectional view of the MME composites. Reproduced from [35] with permission from the Royal Society of Chemistry.

of 0.02 mW cm^{-2} Oe^{-2} at 8 Oe AC magnetic field at the resonance frequency of 60 Hz. The output power was ~1.85 times higher than that of the device without the MFC, 3.33 and 1.17 mW, respectively. A suitable selection of MFC materials could also result in a higher amplification of flux density and maximum output power. However, the authors did not consider the magnet volume during the calculation of the power density of this system, which should be noted when comparing with other ME WPT systems.

Much evidence in the literature argues that combining ME and MME mechanisms could improve the maximum output power. However, most of those investigations have been based on experimental work. There is still a lack of a comprehensive theoretical analysis to understand whether a ME-coupled-MME configuration always significantly outperforms a conventional MME structure, or on which occasions the combination is beneficial. Since the applied magnetic fields interact with both permanent magnet and MS materials, it is difficult to distinguish the contributions of each mechanism in a coupled system if we only analyze the total output power. Answering these questions can provide a deeper insight into the behavior of a ME–MME based system and a guideline to optimize its performance when subject to practical limitations such as device size and available stray magnetic fields.

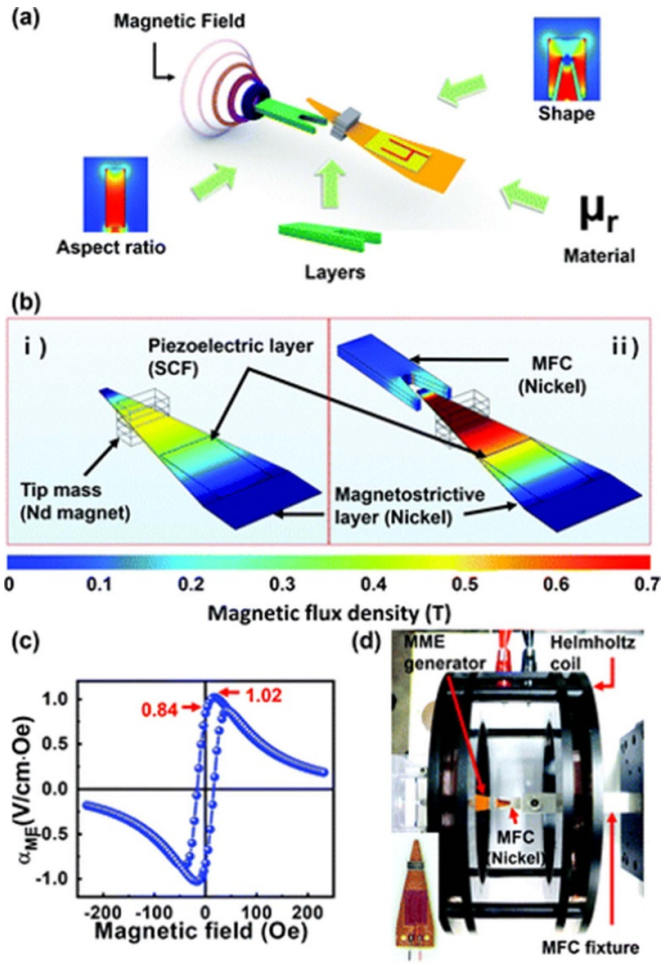

Figure 9. (a) Schematic of the optimization of the MME generator, (b) magnetic flux density simulation with or without the magnetic flux concentrator (MFC), (c) ME voltage coefficient (α_{ME}) of the MME generator, and (d) experimental setup. Reproduced from [36] with permission from the Royal Society of Chemistry.

3.2. ME longitudinal mode

Rather than operating in bending mode, ME longitudinal oscillators consist of ME laminates without proof masses attached to the end and vibrate along their length. The ME longitudinal mode oscillator is a very common, perhaps the most common, ME structure used for WPT. The standard ME longitudinal mode oscillator has a basic structure as shown in figure 10. Most of the ME longitudinal mode structures reviewed in this article either have an externally applied DC bias field or implement a self-biasing mechanism and thus are reviewed in either sections 4 or 5. Here we review a few ME longitudinal mode oscillators that either do not make use of an external DC bias field or are otherwise noteworthy.

O'Handley *et al* [1] presented a ME laminate with three layers Metglas–PZT–Metglas that operates in the longitudinal mode. The ME transducer could produce 2 W cm^{-3} power under an AC magnetic field of 20 Oe and at 60 kHz resonance frequency. Since the applied field strength was relatively high, the ME device was magnetized and excited simultaneously, and therefore, there was no need for the DC bias field for its operation.

A unique longitudinal mode structure was proposed by Li *et al* [38]. The group fabricated a ME composite on a Be–Bronze triangular shaped ultrasonic horn substrate with one Terfenol-D plate and three piezoelectric (PZT) plates as shown in figure 11. Here, three transversely polarized PZT plates (12 mm × 2 mm × 0.8 mm) and one longitudinally magnetized Terfenol-D plate (12 mm × 6 mm × 1 mm) were placed on the same plane and glued on the ultrasonic horn. They demonstrated two times higher ME coefficient than a bilayer composite of the same size (with one PZT and one Terfenol-D plate) at resonance frequency. The high Q ultrasonic horn was used to decrease energy loss and enhance energy density. The authors stated that the vibrating amplitude of the MS Terfenol-D plate can be converged and amplified by the ultrasonic horn due to its shape. They further demonstrate that more vibrating energy can be converted into electricity from either series or parallel connection of three PZT plates than from a single PZT plate [39, 40]. The authors further claimed that the vibrating gain of the ultrasonic horn scales proportionally with the area ratio of the two different cross-sections and is related to its gradient contour and quality factor. Therefore, the ultrasonic horn transfers vibrating energy from the larger cross-sectional area to smaller cross-sectional area and hence an enhancement of power density is achieved. The device can produce 20 μW from a supply of 1 Oe AC and 800 Oe DC bias field. Although, this structure shows higher power output than the bilayer, the volume of this structure is larger and the shape is more complicated than a traditional bilayer.

Bayrashev *et al* [41] proposed a disk shaped (7 mm diameter) ME laminate with Terfenol-D–PZT–Terfenol-D for use as a biomedical implant. This is a free standing bulk oscillator, but oscillates in thickness mode rather than longitudinally. A NdFeB permanent magnet with a diameter of 25.4 mm is used to generate the magnetic flux change by attaching it to the shaft of a linear variable frequency (1–30 Hz) dc motor. They claimed this approach as a low frequency method of powering microsystems. Their reported power is around 80 μW, which is reasonable for a biomedical implant. However, from their reported values, it is difficult to understand the precise magnitudes of the AC and DC magnetic fields to which the laminate, and therefore the person in which the device is implanted, is exposed.

3.3. ME bending mode

In contrast to ME longitudinal mode oscillators, ME bending mode oscillators are typically two-layer structures: one MS layer and one piezoelectric layer. Thus, the magnetically generated force in the MS layer causes a bending mode oscillation. Even if the structures have more than two layers, they are asymmetric through the thickness such that a bending mode results from applied AC magnetic fields.

Chlaihawi *et al* [42] developed a screen-printed self-biased laminate that exhibited a power density of 639.6 μW cm^{-3} under an AC magnetic field of 92 Oe at a frequency of 100 Hz with an optimal load of 100 kΩ. The device was fabricated by

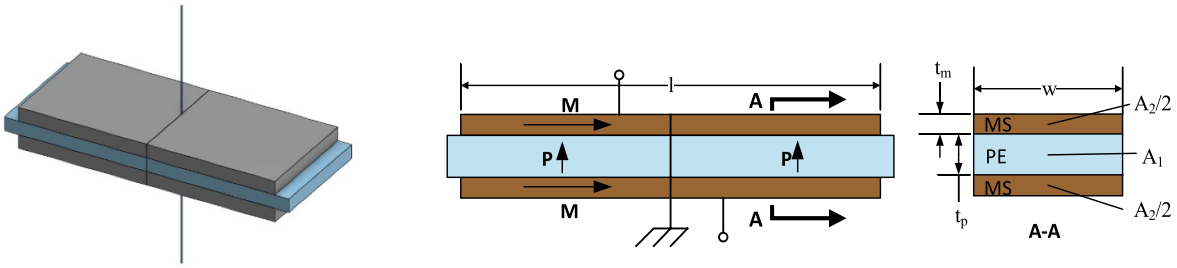

Figure 10. Standard geometry for ME longitudinal model oscillator. Blue layer center layer is piezoelectric. Brown outer layers are MS. The structure is typically either mounted along its center line allowing free vibration to either side or free standing [37].

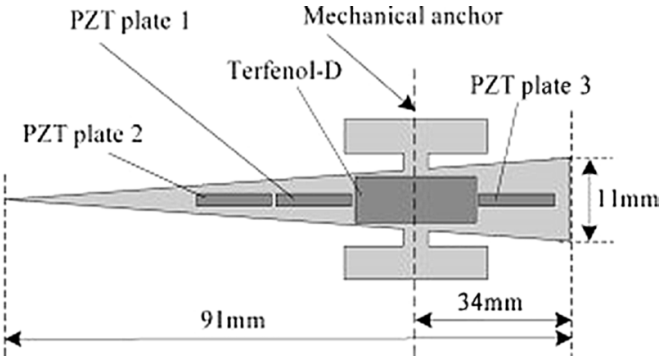

Figure 11. Composite comprised of Terfenol-D, PZT and ultrasonic horn. Reprinted from [38], Copyright (2010), with permission from Elsevier.

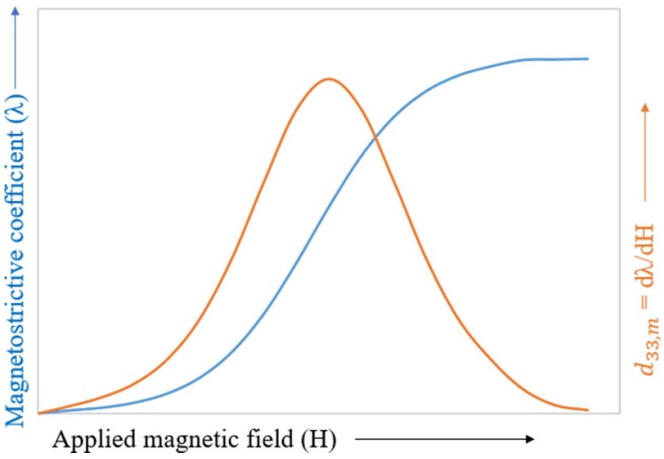

Figure 12. Relation between MS coefficient (λ), $d_{33,\mathrm{m}}$ and magnetic field.

screen printing PVDF on a Metglas substrate. Ag ink was also printed on top of the PVDF layer as electrodes for the ME–MME transducer. The fabrication method is cost-efficient, light weight and can increase the flexibility of a ME laminate. It was not reported whether the device operated at resonance of off-resonance. The authors did not clarify whether the prototype requires a DC bias field for its operation. However, with a high AC field applied, the Metglas could be magnetized and excited at the same time.

Asymmetric ME laminated composites operating in bending mode at low-frequency ranges have been thoroughly investigated theoretically in the literature [43, 44]. However, the performance of the bending vibration was shown to be worse than that of the longitudinal mode (i.e. usually compared in terms of the ME coefficient) [45, 46]. Therefore, the bending mode operation is less favorable for a ME-based wireless power transfer system (WPTS) when compared to ME–MME and ME longitudinal mode structures.

4. Approaches to magnetic field biasing

In this section, we discuss different approaches of applying an external DC magnetic field bias to improve the performance of ME laminates. A DC magnetic bias superimposed on an AC magnetic field enables operation closer to saturation magnetostriction [47]. This DC magnetic field magnetizes the MS materials by aligning their randomly oriented magnetic domains in one direction. Under the influence of a superimposed AC magnetic field, rotation or reorientation of the magnetic domains causes internal strain in the material structure (i.e. magnetostriction). The resulting strain depends on the degree of the material's base structure homogeneity and the material formulation. The strains in the structure lead to the stretching (positive magnetostriction), or contraction (negative magnetostriction) of the material in the direction of the magnetic field [48]. The primary means of applying a DC magnetic field bias are to place a magnet (permanent magnet or electromagnet) near the device under test, or to place the device under test in a DC Helmholtz coil.

Truong and Roundy [8] experimentally and analytically showed that magneto-mechanical transduction factor ($\Gamma_{\mathrm{m}} = -2wt_{\mathrm{m}}\frac{d_{33,\mathrm{m}}}{s_{33}^{\mathrm{H}}}$) limits the maximum power available for transfer to a resistive load. Γ_{m} is a function of the piezomagnetic constant $d_{33,\mathrm{m}}$, which is a function of DC bias ($d_{33,\mathrm{m}} = d\lambda/dH_{\mathrm{DC}}$) as shown in figure 12. Power can be optimized by maximizing the piezomagnetic constant which can be achieved by applying the correct DC bias. Truong and Roundy found 133 Oe optimum DC bias for their Galfenol–PZT–Galfenol longitudinal mode oscillator structure which they applied with external (i.e. not attached to the ME structure) permanent magnets. Under this DC bias and an applied AC magnetic field of 3 Oe their reported output power is around 10 mW at 70.47 kHz resonance frequency.

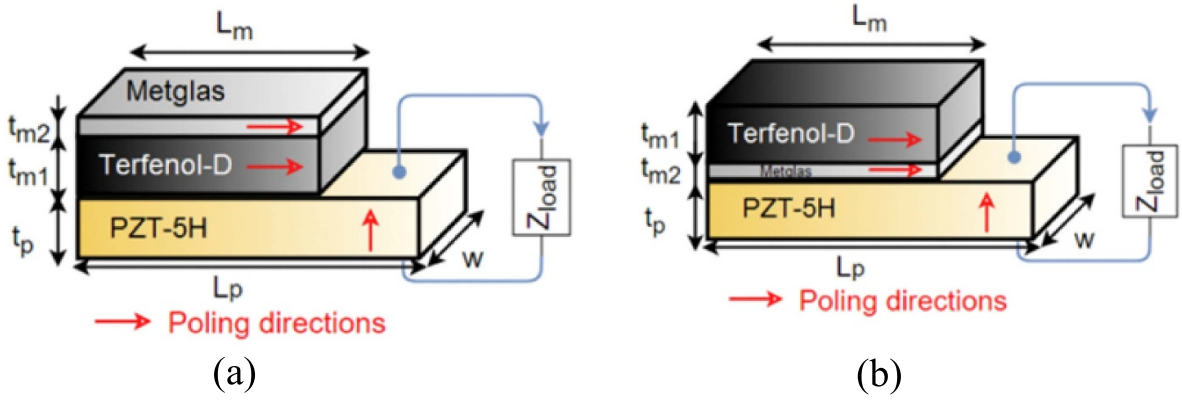

Figure 13. Trilayer ME structures: (a) Metglas–Terfenol-D–PZT–5H, and (b) Terfenol-D–Metglas–PZT. Reprinted from [55], Copyright (2019), with permission from Elsevier.

Bian *et al* [49] fabricated a symmetric FeNi–PZT–FeNi longitudinal mode oscillator structure which operated under 0.3 Oe root mean square (RMS) AC magnetic field and an optimal DC bias of 50 Oe. The DC magnetic bias is applied by using a pair of annular permanent magnets (Nd–Fe–B). Under this condition their reported output power is 0.956 mW cm^{-3} for an optimal load of 25 kΩ and 26.8 kHz resonance frequency. Despite having a low piezomagnetic constant, this longitudinal resonator achieved a high ME coefficient (376 V cm^{-1} Oe^{-1}).

The optimum bias magnetic field mainly depends on the material properties of the MS material used. Researchers have demonstrated that higher optimum bias is needed for Terfenol-D than nickel, FeNi alloy or Galfenol. Wang *et al* [50] investigated a trilayer ME device with Terfenol-D–PMN–PT–Terfenol-D and found an optimal DC bias of 400 Oe DC which they applied with a U-shaped electromagnet. The device produced 1.9 mW Oe^{-1} power output under 1 Oe AC field. Wang *et al* [51] also explained how the optimum bias field causes maximum strain and minimum stiffness and how increasing or decreasing the bias field from the optimum causes a corresponding decrease in strain and increase in stiffness.

Rizzo *et al* [52] proposed a disk-shaped trilayer ME structure with Terfenol-D–PZT–Terfenol-D which also exhibits optimum power at high optimum DC bias. The authors chose disk-shaped pieces because they wanted to avoid unwanted electromagnetic effects which may occur at the angles of FM structures. They supplied 1000 Oe bias field by using an electromagnet and reported 175 mW cm^{-3} output power under 15 Oe RMS AC field and 200 kHz resonance frequency for 470 Ω optimum loading. The group claimed that their device can be used as a medical implant. Their reported optimum power output is very high, however this is under a very large AC magnetic field and power scales with the square of the AC magnetic field. We also note that this AC magnetic field amplitude is well above suggested safety limits for biomedical implants [53, 54].

Malleron *et al* [55] experimentally showed the effect of a Metglas layer on ME composites of Terfenol-D/PZT–5H with different configurations as shown in figure 13. They investigated four structures, Metglas–PZT, Terfenol-D–PZT, Terfenol-D–Metglas–PZT and Metglas–Terfenol-D–PZT and found that the Terfenol-D–Metglas–PZT composite performs better than the others. They explained that if Metglas is placed between the bulk Terfenol-D layer and the piezoelectric layer, it improves the mechanical energy transfer by concentrating stress near the piezoelectric layer. Their reported power output for the Terfenol-D–Metglas–PZT–5H composite is 600 μW under 1 Oe AC field at 70 kHz and 682 Oe DC magnetic field supplied by an external magnet. Although they did not find any significant effect on required optimum bias magnetic field due to adding a thin amorphous Metglas layer with Terfenol-D, they did get better output power by adding the Metglas. As Metglas is a high permeability material, it concentrates the induction magnetic flux. The authors claimed that as Metglas concentrates the magnetic induction flux and stress near the PZT in a Terfenol-D–Metglas–PZT composite, they achieved higher power and a higher ME coefficient than the other composite configurations. But this is not always true for other materials. Mandal *et al* [56] found a lower ME coefficient for a Ni–Metglas–PZT composite than for a Metglas–Ni–PZT composite. Therefore, the exact relationship between the composite configuration and ME coefficient and power output is still uncertain. However, these experimental results open an exciting question regarding how to combine various MS materials for a ME WPTS.

Onuta *et al* [57] developed an all-thin-film ME composite on silicon cantilever. The devices were fabricated on a silicon oxide/nitride/oxide stack. The ME cantilevers were composed of $Fe_{0.7}Ga_{0.3}$ as the MS phase and $Pb(Zr_{0.52}Ti_{0.48})O_3$ as the piezoelectric material [57]. A peak power density of 0.7 mW cm^{-3} (RMS) was measured at a resonance frequency of 3833 Hz and with an optimal load of 12.5 kΩ. The DC bias field and AC field (applied by nested Helmholtz coils) were 66.1 Oe and 1 Oe (RMS), respectively. This result showed that thin film structures under consideration can perform equally as bulk structures. More interestingly, under zero DC magnetic field bias, the ME coefficient was only 20% less than that with the optimal DC bias field. This implies a 36% reduction in power output with no DC bias. This despite the fact that there is no explicit self-biasing mechanism applied.

Reis *et al* [58] manufactured a Metglas–PVDF–Metglas composite which requires a much lower DC bias than other MS materials like Galfenol or Terfenol-D. Their reported output power is 0.9 mW cm^{-3} under 0.4 Oe AC and 7 Oe DC bias field applied by Helmholtz coils at 54.5 kHz resonance frequency with 180 kΩ optimum loading. The authors mainly focused on the electronic optimization of the energy harvesting system which is out of the scope of this review. Previously Lasheras *et al* [59] also fabricated a similar Metglas–PVDF–Metglas laminate and showed how the length of the laminate impacts the power output, DC bias, resonance frequency, and ME coefficient (α_{ME}). Output power and α_{ME} increase and the required optimum DC bias and resonance frequency decrease with increasing length of the laminate. Because Metglas has an extremely high permeability, short composites suffer the strong effects of demagnetization fields. Therefore, it is not surprising that longer devices produce more power and voltage. The authors did not explain why the DC bias fields decrease with the increase of the length. Although a longer laminate gives more power and needs a smaller DC bias for optimum operation, the interest in fabricating miniature devices may limit the length achievable in many WPT applications.

Recently, ME laminates are increasingly being investigated in the field of WPT for biomedical implants because of their favorable size/power relationship [60–63]. Miniature ME devices can outperform coupled inductive devices for WPT in biomedical implants [62]. Singer *et al* [63] fabricated millimeter-sized asymmetric devices with Metglas and PVDF for wireless neural simulations. The system is designed with permanent magnets for supplying the 80–90 Oe DC bias and an electromagnetic coil to supply 10 Oe or 20 Oe AC field at the resonance frequency. They manufactured two different sized (20 mm^3 and 4 mm^3) ME laminates. The 20 mm^3 (resonance frequency 171 kHz) and 4 mm^3 (250–400 kHz) laminates produce around 0.1–0.2 mW power and 2 mW power respectively. The authors focus mostly on neural simulations and so their analysis of power is incomplete. Although these implants produce mW range power, they applied very high AC magnetic fields which may cause safety concerns for biomedical implants. The ME device used a permanent magnet placed near the end of the Metglas to create the DC bias. It should be noted that the use of a permanent magnet may cause size and safety issues for a biomedical implant. Finally, Park *et al* [64] proposed ME laminates for biomedical implants composed of lead free piezoelectric single crystal, BCT–BZT $(82BaTiO_3 - 10BaZrO_3 - 8CaTiO_3)$ and Ni plates that have comparable power output density to lead based piezoelectric ME laminates. This approach may provide increased safety given the elimination of lead in the piezoelectric material.

Newacheck and Youssef [65] proposed two ME laminates with different geometries to wirelessly power small electronic devices. Two ME composites, one circular and the other rectangular, have been made with Terfenol-D and PZT layers. They perform two tests by using the circular laminate as a transmitter and the rectangular laminate as a receiver and vice versa. A 100 μW power can be transferred at resonance by their system under an AC magnetic field of 1.4 Oe RMS and an optimum DC bias of 500 Oe applied by an electromagnet. The experimental setup is shown in figure 14. The authors clearly show the effect of DC bias and geometry of the laminate on the ME coefficient. This approach to WPT is different than others because they use ME composites both for transmitting and receiving, which they call bi-directional ME WPT.

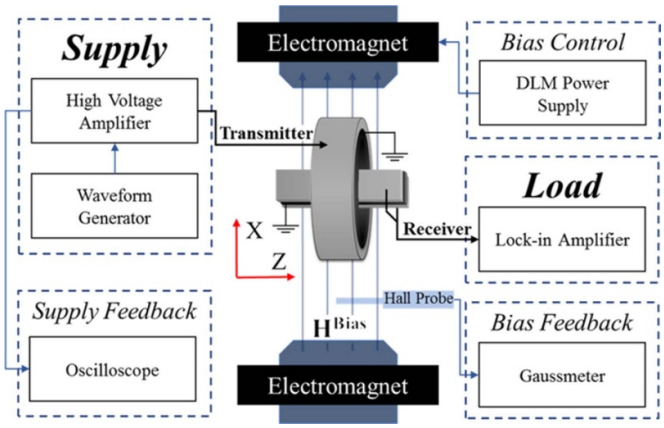

Figure 14. WPT experimental setup with a concentric ring ME transmitter and laminate plate ME receiver. Reproduced from [65].

Li *et al* [66] designed a ferro-nickel (Fe–Ni)/PZT H-type fork ME structure and an energy management circuit for energy harvesting. The H-type fork ME composite structure is composed of two same-size-rectangular composites as shown in figure 15. The device would be classified as a ME longitudinal mode oscillator, but we note that it is a unique configuration. The Fe–Ni alloy is magnetized along the longitudinal direction. The PZT–8H is polarized along the thickness direction. The same identical vibrating waves from the two beams are induced and superimposed due to the symmetrical fork structure. The output power for the resonant fork composite structure was 61.64 μW at an AC magnetic field of 0.2 Oe and a DC bias field of 100 Oe. The authors experimentally showed that the resonant fork composite configuration exhibited a higher ME coefficient compared to that of the conventional traditional structure. This is primarily due to the fact that the active material volume used in the H-type prototype was twice as much as that in the traditional beam.

5. Self-biased ME structures

ME laminates typically need a DC bias in addition to an AC magnetic field for optimum performance. As detailed in the previous sections, the bias field is often supplied by a magnet attached to the tip of the ME structure (as in the ME–MME configuration discussed in section 3.2), by a nearby permanent magnet, by an electromagnet, or by a Helmholtz coil. Use of a permanent magnet mass alters the dynamics of the device and can make the device too large or unsafe (e.g. in the case of biomedical implants) for many applications. Use of biasing magnets (permanent magnets or electromagnets) is impractical in many if not most real applications. Therefore, researchers have taken various approaches to fabricate self-biased ME

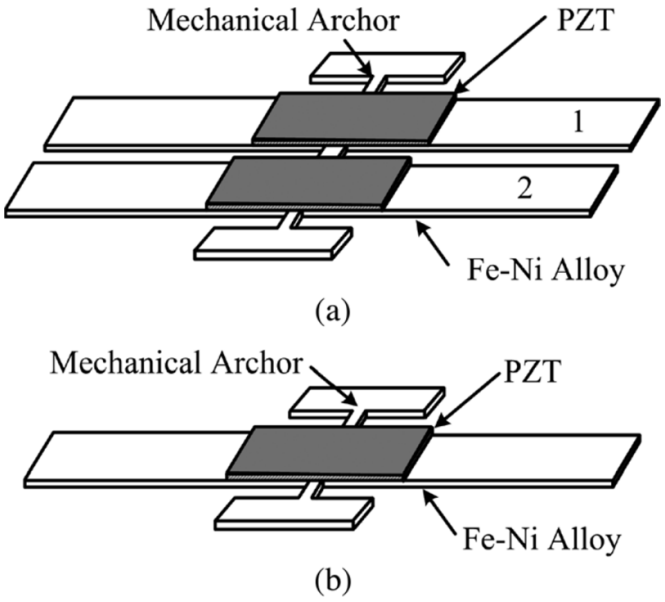

Figure 15. ME composite structure: (a) H-type fork ME composite structure, and (b) rectangular ME composite structure. © [2011] IEEE. Reprinted, with permission, from [66].

laminates [67]. Some researchers using magnet masses at the tip of the ME beam and classified them as self-biased devices [68]. However, for the purposes of this paper, we consider a self-biased device one that does not use any kind of permanent magnet (i.e. magnetic mass which is not MS) or external DC bias for the ME effect. In other words, if the bias field (actual magnetostatic field or effective field as in the case of exchange bias) is produced by the MS material itself, even if that material is a hard magnetic material with remanent magnetization, then we consider it a self-biased ME laminate. Although, we acknowledge this is our own classification, and not one that is universally accepted in the literature. In this section, we discuss self-biasing approaches in order to critically compare these different approaches for WPT. Most of the self-biased papers have compared their laminate performance on the basis of the ME coefficient ($\alpha_{\mathrm{ME}} = V/(t_{\mathrm{p}}H_{\mathrm{ac}})$).

5.1. Self-biasing by pre-magnetizing MS layers

Magnetization of MS materials can result in an enhanced MS effect with no external bias by virtue of the fact that the remanent magnetization serves to magnetically bias the device. Pre-magnetization is accomplished using multiple methods. Some materials will maintain a significant remanent magnetization at room temperature when subjected to large DC magnetic fields. In some cases, magnetic annealing enhances the remanent magnetization in the direction of the field applied during annealing. This type of self-biasing field is sometimes referred to as an anisotropy field, such as in [22], because of the resulting anisotropic magnetic properties of the annealed MS material. (Note that exchange anisotropy is a different effect that will be discussed under section 5.3.) In either case, the result is a large remanent magnetization in the MS material that serves as its biasing field.

Kambale *et al* [69] built symmetric (trilayer) and asymmetric (bilayer) ME structures with Ni ($30 \times 17 \times 0.25$ mm^3) and piezoelectric macrofiber composites (MFCs) and experimentally investigated their performance. They achieved self-biased operation by virtue of the fact that the Ni layer retained some remanent magnetization (i.e. it was pre-magnetized). The reported self-biased ME coefficients ranged from 0.016 to 0.25 V cm^{-1} Oe^{-1} depending on device structure (i.e. asymmetric or symmetric) and orientation. Under an experiment in which the ME devices were placed on a magnetic stirrer and therefore subjected to both mechanical vibrations and AC magnetic fields, the authors reported a power output of 6.2 μW and 0.1 μW for Ni/MFC and Ni/MFC/Ni laminates, respectively. However, since the operating frequency used in these experiments was far away from the resonance frequencies of each structure, and the load resistances used were not optimal, it is difficult to evaluate and compare the maximum output power these generators can provide.

Many researchers have used Metglas to fabricate self-biased laminates as it needs a relatively low DC bias for its optimum performance [70, 71]. The main concern is how to supply the small DC bias without the use of external magnets. Ma *et al* [72] proposed magnetic annealing of Metglas in order to permanently magnetize it. Magnetic annealing of Metglas introduces a nano-crystal phase into the amorphous material with the resulting effect that the Metglas behaves as a hard magnetic material (i.e. exhibits a larger hysteresis loop). They annealed the Metglas with a magnetic field applied in the longitudinal direction at various temperatures and times to optimize the performance. They found that a magnetic field of 3000 Oe at 350 °C for 5 min resulted in optimum performance. They then use this annealed Metglas (10 mm × 5 mm × 25 mm) to fabricate a Metglas–PZT–Metglas laminate. This laminate produced a voltage 1.3 V ($\alpha_{\mathrm{ME}} = 15.5$ V cm^{-1} Oe^{-1}) at 146.4 kHz resonance frequency under a 3 Oe AC magnetic field and zero DC bias field. Although a successful approach for self-biased laminates, the careful optimization of magnetic annealing field, timing, and annealing medium (vacuum, air, nitrogen) make this process complex. An additional significant drawback of this process is that magnetic annealing makes the Metglas very brittle [73].

To overcome the drawbacks of the above procedure the same authors suggested another approach of integrating a hard magnetic layer with the ME laminates [74]. They used a hard magnetic ribbon composite, SFO ($SrFe_{12}O_{19}$), with a large coercive field and unannealed Metglas to fabricate their laminate. The SFO–Metglas–PZT–Metglas–SFO laminate produced 29 V cm^{-1} Oe^{-1} under 120 kHz resonance condition and zero bias field. The authors stated that as the SFO ribbon has higher coercivity than annealed Metglas, it creates a larger magnetostatic field inside the Metglas compared to the remanent magnetization of the annealed Metglas in [72]. They further showed that by changing the thickness of the SFO ribbon, the magnetostatic field can be optimized for better output. According to our definition, this approach is not a self-biased laminate as the SFO ribbon is not significantly magnetostrictive. The SFO layer simply induces a magnetostatic field in the MS material. Thus, we would classify this approach as a

method to apply a DC bias field. We include it here as it is part of a body of work from Ma *et al*.

Zhang *et al* introduced self-biased ME laminates that make use of Samfenol ($SmFe_2$) due to its large internal anisotropy. (Note, the authors refer to the large remanent magnetization of the Samfenol layer as a large anisotropic field because of Samfenol's inherent magnetic anisotropy.) In [22] the authors manufactured $SmFe_2$–PZT–$SmFe_2$ composites. The $SmFe_2$–PZT–$SmFe_2$ laminate produced $\alpha_{ME} = 39.5$ V cm^{-1} Oe^{-1} under 1 Oe AC magnetic field at zero bias and resonance (119.75 kHz). In another device [75], the authors introduced a self-biased trilayer ME laminate heterostructure that consists of positive (Terfenol-D) and negative ($SmFe_2$) giant MS materials and piezoelectric ceramics. This ME composite was able to generate a maximum power of 0.323 μW with a 2.6 MΩ load resistance under an applied AC magnetic field of 1 Oe at an anti-resonance frequency of 111.5 kHz. The self-biased operation results from the opposite magnetically induced stresses from the top layer (Terfonol-D) and the bottom layer ($SmFe_2$).

5.2. Self-biasing by magnetization grading

Magnetization grading results from bonding together two or more dissimilar MS materials (i.e. different saturation magnetizations). This grading of magnetic properties can result in a large piezomagnetic constant under zero bias. As described in [76, 77] when two different MS materials are bonded together, a magnetic field will be induced in the transverse direction and this field will be antiparallel to the gradient of their magnetization (∇M). As the applied AC magnetic field is typically along the length or width of the ME device, the field resulting from the magnetization grading is orthogonal to the applied AC field. The large piezomagnetic constant is a result of the moment of rotation acting on the magnetic layers in response to the applied AC field (see Mandal *et al* [56]). The difference in saturation magnetizations can be achieved by choosing MS materials with different permeability and coercive fields.

Mandal *et al* [56] used two different MS materials (annealed nickel and Metglas) and bonded them with PZT to make self-biased ME laminates. Due to the difference in saturation magnetizations of Metglas and nickel, a transverse magnetic field is induced. Their experimental results show $\alpha_{ME} = 46$ V cm^{-1} Oe^{-1} at 170 Hz resonance frequency under 1 Oe AC magnetic field. (Note, this is a ME bending mode device rather than a ME longitudinal mode device.) Their optimized α_{ME} value is for a laminate with lateral dimensions of 5 cm × 1 cm. They optimized the α_{ME} value by changing only the Metglas layer thickness. A critical point to note here is that they pre-magnetized their virgin sample before taking the zero-bias measurements. Thus, the nickel layer maintains a remanent magnetization that increases the magnetization grading effect and may also increase the piezomagnetic constant of the nickel itself. It is not always clear which effect is contributing more to the self-biased performance, but this potential combination of effects is common for many magnetization graded devices.

Another approach of magnetization grading has been presented by Li *et al* [78]. They laminated annealed Metglas and unannealed Metglas together to create the magnetization grading which they bonded to the PZT layer to create a ME device. Then they pre-magnetized the laminate by using 2 kOe magnetizing field. Due to the difference in saturation magnetizations of crystalline annealed Metglas and amorphous unannealed Metglas, a magnetostatic field is induced inside the laminate and this internal bias field causes the zero-bias performance. Their 80 mm × 10 mm self-biased laminate was able to produce 380 V cm^{-1} Oe^{-1} under 0.1 Oe AC magnetic field and at 33.7 kHz resonance frequency with zero DC bias. Although annealed Metglas is difficult to handle due to its brittleness, this approach is a good example of self-biased laminates with high α_{ME} and high output voltage.

Following the magnetization grading approach, Chen *et al* [79] fabricated three types of self-biased laminates and compared their performance: FeCuNbSiB–Ni–PZT (FeNiP), FeCuNbSiB–FeNi–PZT (FeFP) and FeCuNbSiB–Terfenol-D–PZT (FeMP). They first performed low frequency analysis by varying the DC bias supply from −500 Oe to 500 Oe under 1 Oe AC magnetic field supply. In addition to characterizing the devices, this step likely also pre-magnetized some of the MS layers. From this low frequency analysis, they found very low α_{ME} (around 17.25 mV cm^{-1} Oe^{-1} for FeNiP) at zero bias. They performed the same analysis at resonance and found a higher value of all three laminates due to the high mechanical quality factor. The FeNiP laminate produced a higher $\alpha_{ME} = 126.6$ V cm^{-1} Oe^{-1} at 154 kHz resonance frequency and at zero bias compared to the other two laminates. Xu *et al* [80] also created magnetization graded laminates by combining high permeability FeCoV foils and Terfenol-D. They reported a zero biased $\alpha_{ME} = 19.6$ V cm^{-1} Oe^{-1} at 115.1 kHz resonance frequency.

Continuing from their prior work [22, 75], Zhang *et al* [81] demonstrated a similar principle by manufacturing a $SmFe_2$–Terfenol-D–PMN–PT–Terfenol-D–$SmFe_2$ laminate. Their laminate produced 13.75 V cm^{-1} Oe^{-1} at 97.5 kHz resonance frequency at zero bias. According to the authors, the induced internal bias field (H_{int}) inside the laminates is the summation of two fields: one is induced by the magnetic property mismatch of the two giant MS materials (i.e. magnetization grading), and the second is induced by the internal anisotropic field (i.e. remanent magnetization) of Samfenol. Note, the terminology in this paper seems to be somewhat different than in other papers in this review. The authors refer to the field resulting from the different magnetic properties of Samfenol and Terfenol-D as 'exchange biasing'. However, we believe that this is more properly referred to as magnetization grading.

Following the insights from these previous works on magnetization grading, we manufactured five-layer (Metglas–Ni–PZT–Ni–Metglas) self-biased laminates. We have characterized the effect of remanent magnetization of the nickel layer on the laminates' self-biased performance and reported their power output at low AC magnetic field [82]. In our devices, the self-biasing effect is likely the caused by the combined effect

of the remanent magnetization in the Ni layer and the magnetization grading effect of the two magnetically mismatched layers (Metglas and Ni). We have verified that without pre-magnetization of the laminates, the self-biased effect is significantly diminished. Similarly, even with pre-magnetization, the self-biased performance of a Ni–PZT–Ni laminate is weak. Therefore, the combination of different MS materials and pre-magnetization is important for good self-biased performance. Our self-biased device can produce around 250 μW power at 1.3 Oe AC magnetic field at resonance (188 kHz), which is reasonable to power a range of biomedical implants.

As a final note, most of the self-biased laminates discussed make use of a hard magnetic MS material that is pre-magnetized. The stability issues of the laminates have not yet been researched extensively. First, the remanent magnetization can degrade over time, especially if subjected to high temperatures. Second, there is a possibility of degrading the remanent magnetization during cycling with the magnetic fields if the AC fields approach or are higher than the remanent magnetization. This effect is unlikely if the AC magnetic field is within the μT range. To our knowledge these stability issues have not been reported on in the context of self-biased ME devices.

5.3. Self-biasing mechanism by exchange biasing

Exchange bias refers to the shift in the hysteresis loop of FM/antiferromagnetic (AFM) bilayers. As explained by Stamps [83], FM materials tend to have a large exchange parameter (i.e. high ordering) but low anisotropy. AFM materials tend to have large anisotropies but low ordering. When the materials are brought together, exchange coupling between the materials can result in FM behavior with stable order and high anisotropy. The phenomenon is referred to as exchange bias because the hysteresis loop of the FM/AFM system can be centered around a non-zero magnetic field. (Note, we refer to this effect as exchange bias, but it is sometimes referred to as exchange anisotropy.) This effect has been widely exploited in magnetic recording. The process for making exchange biased heterostructures is detailed in [84, 85].

To our knowledge, only one group has published work applying exchange biasing to ME laminates. The composites presented by Lage *et al* [86] are composed of piezoelectric AlN (aluminum nitride) and multilayers of Ta/Cu/$Mn_{70}Ir_{30}$/$Fe_{50}Co_{50}$ or Ta/Cu/$Mn_{70}Ir_{30}$/$Fe_{70.2}Co_{7.8}Si_{12}B_{10}$ as MS layers. The composite with $Fe_{70.2}Co_{7.8}Si_{12}B_{10}$ is able to produce $\alpha_{ME} = 96.7$ V cm^{-1} Oe^{-1} under 1 Oe AC magnetic field supply at zero bias and at resonance. Although, the α_{ME} value of this self-biased composite is high, the output voltage is very low (19.34 mV) because the AlN layer is very thin. Lage *et al* [87] again tried to improve the performance (in terms of α_{ME}) of the laminates by increasing the thickness of the multilayers. The resulting 25 mm long laminate produced a higher α_{ME} of 430 V cm^{-1} Oe^{-1}. However, the output voltage is still in the mV range. At their current state, these exchange-biased laminates do not compare well with other approaches for ME WPT. However, they may be a good choice for self-biased sensing applications. Analyzing the stability issues and exploring different materials for the multilayers to improve the performance would be good future research topics.

Most papers on self-biased ME laminates are primarily interested in the α_{ME} value as the relevant figure of merit. Although this is appropriate for the sensing application, α_{ME} does not directly translate to better performance as a WPT receiver. α_{ME} is normalized by the thickness of the piezoelectric layer and the applied AC magnetic field. Received power, however, does not scale in the same way as α_{ME}. (For a further treatment of the relationship between α_{ME} and received power, we refer the reader to [8].) Therefore, we next compare different ME WPT receivers based on a new power figure of merit.

6. Figures of merit and comparative analysis

This section compares the previously reported ME structures based on different figures of merit, including our suggested ME WPT power figure of merit. As discussed in the previous section, the ME coefficient, $\alpha_{ME} = V/t_p H_{ac}$, is not a perfect figure of merit for WPT applications. α_{ME} is most applicable to a sensing application in which the voltage magnitude, not power, is the critical factor. Other common figures of merit include power density (mW cm^{-3}) and power density normalized by the square of the applied magnetic field (mW cm^{-3} Oe^{-2}). This last power density does correctly account for the square of the applied magnetic field, however it neglects frequency. Based on prior work, the following relationships hold, and should inform the relevant power figure of merit:

$$\text{Power} \propto \text{volume}$$

$$\text{Power} \propto H_{ac}^2$$

$$\text{Power} \propto \text{frequency}.$$

For a further discussion of the relationship between power and volume, and power and AC magnetic field (H_{ac}) we refer the reader to [8]. For a further discussion of the relationship between power and frequency we refer the reader to [88]. For inductively coupled WPT it is commonly stated that power scales with frequency squared, which is true under certain idealized conditions. (A full discussion of power scaling for inductively coupled WPT is beyond the scope of this paper.) However, Truong [88] has shown that for ME WPT receivers, the relevant scaling for ME WPT is linear with frequency assuming a constant quality factor. Therefore, we propose the following power figure of merit:

$$\text{FOM}_P = \frac{P}{\text{vol}\, H_{ac}^2 f} \tag{4}$$

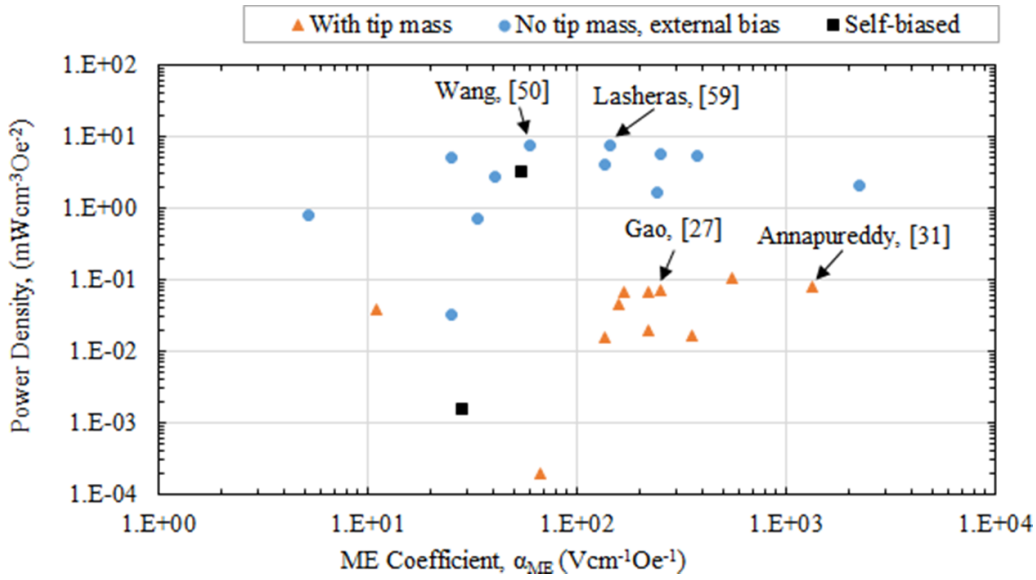

Figure 16. Relationship between power density and α_{ME}.

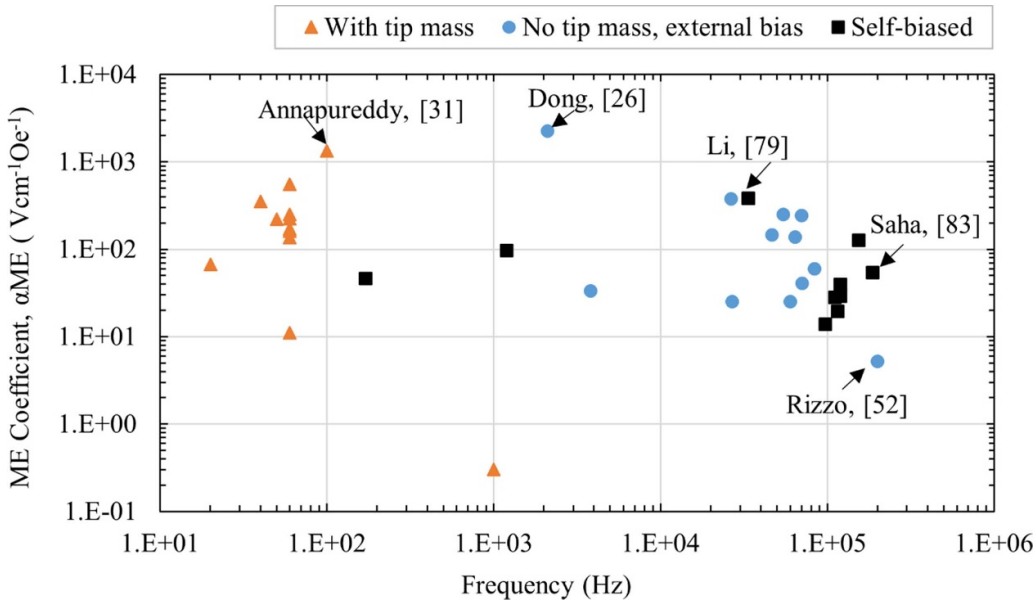

Figure 17. Relationship between α_{ME} and operating frequency.

where FOM_P is the power figure of merit, P is the measured output power, vol is the total device volume including permanent magnets or auxiliary structures if present, H_{ac} is the applied AC magnetic field, and f is the operating frequency in Hz. The units we use for this power figure of merit are mW cm^{-3} Oe^{-2} Hz^{-1}. This power figure of merit is useful in comparing different mechanical structures, approaches to external biasing, and self-biasing approaches. We should note that we calculate power density and FOM_P by calculating the total volume of the ME structures with the volume of the tip magnetic mass. Some authors only calculate power density based on the active volume of the ME laminate and do not consider the structure's full size. Furthermore, some authors do not consider the magnet volume for ME–MME structures. Where possible we have tried to correct for this to make fair comparisons.

We classify ME WPT structures into three categories: ME devices with tip magnetic masses, ME devices with external DC bias, and self-biased ME devices. We first plot relationships between relevant parameters (α_{ME}, power density, FOM_P, and frequency) in figures 15–18 for these three categories to further investigate the validity of FOM_P. We then list the relevant parameters of a wide range of publications reviewed herein in tables 3–5.

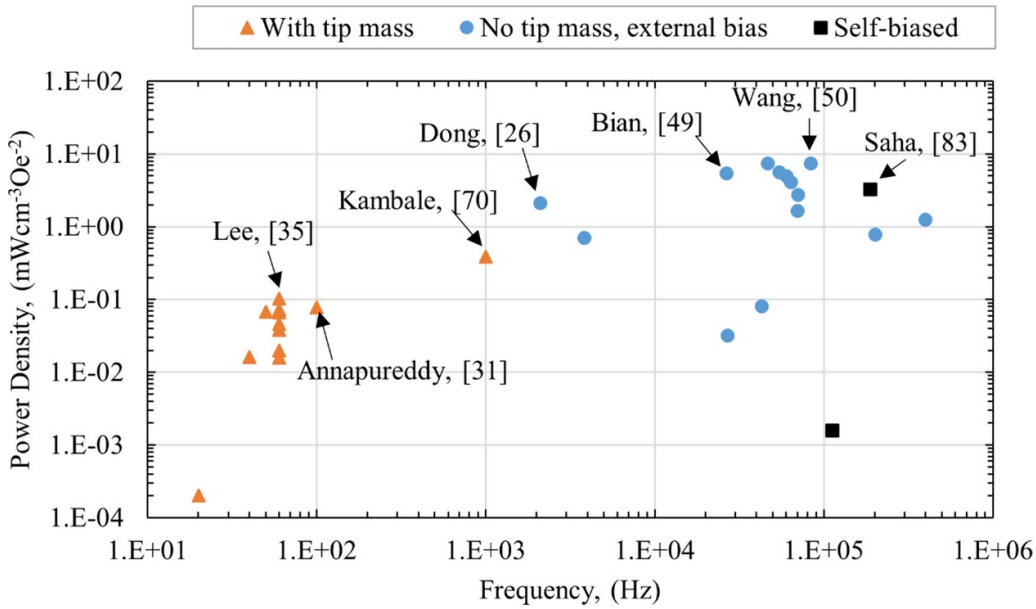

Figure 18. Relationship between power density normalized by the square of the magnetic field and applied frequency.

Table 3. ME WPT with tip mass.

Author	Year/reference	α_{ME} V cm^{-1} Oe^{-1}	Power density mW cm^{-3} Oe^{-2}	Frequency Hz	FOM$_p$, mW cm^{-3} Oe^{-2} Hz^{-1}
Dong	2008/[26]	66.67	2×10^{-4}	20	1×10^{-5}
Gao	2012/[27]	250	7.2×10^{-2}	60	1.2×10^{-3}
Kambale	2014/[69]	0.3[a]	3.8×10^{-1}	1000[a]	3.8×10^{-4}
Ryu	2015/[28]	160	4.6×10^{-2}	60	7.6×10^{-4}
Annapureddy	2016/[29]	135.5	1.5×10^{-2}	60	2.6×10^{-4}
Annapureddy	2016/[30]	353	1.6×10^{-2}	40	4×10^{-4}
Annapureddy	2018/[31]	1330	7.8×10^{-2}	100	7.8×10^{-4}
Kang	2018/[32]	11	3.7×10^{-2}	60	6.3×10^{-4}
Lu	2019/[33]	220	6.7×10^{-2}	50	1.3×10^{-3}
Chlaihawi	2016/[42]	—	7.5×10^{-5}	100	7.5×10^{-7}
Sriramdas	2020/[34]	222.4	1.9×10^{-2}	60	3.3×10^{-4}
Lee	2020/[35]	557	1×10^{-1}	60	1.7×10^{-3}
Song	2020/[36]	170	6.5×10^{-2}	60	1.1×10^{-3}

[a] Off-resonance values.

As shown in figure 16, there does not seem to be any clear relationship between power density and α_{ME}. Here, if we consider the systems with tip masses, we can see that Gao *et al* [27] and Annapureddy *et al* [31] have very different α_{ME} values, but similar power densities (α_{ME} = 250 V cm^{-1} Oe^{-1}, power density = 7.2 × 10^{-2} mW cm^{-3} Oe^{-2} for Gao *et al* [27] and α_{ME} = 1330 V cm^{-1} Oe^{-1}, power density = 7.8 × 10^{-2} mW cm^{-3} Oe^{-2} for Annapureddy *et al* [31]). Again, if we consider the systems with external bias we can see that the power density values do not depend on α_{ME} values (α_{ME} = 60 V cm^{-1} Oe^{-1}, power density = 7.4 mW cm^{-3} Oe^{-2} for Wang *et al* [50] and α_{ME} = 145.6 V cm^{-1} Oe^{-1}, power density = 7.3 mW cm^{-3} Oe^{-2} for Lasheras *et al* [59]). Therefore, it is evident that α_{ME} values do not have any specific relationship with power density of the ME WPT systems and device performances cannot be judged by the α_{ME} values alone.

Figure 17 plots the relationship between α_{ME} and operating frequency. If we consider Annapureddy *et al* [31] (α_{ME} = 1330 V cm^{-1} Oe^{-1} and Frequency = 100 Hz), Dong *et al* [26] (α_{ME} = 2250 V cm^{-1} Oe^{-1} and Frequency = 2100 Hz) and Li *et al* [78] (α_{ME} = 380 V cm^{-1} Oe^{-1} and Frequency = 33 700 Hz), we see that there is no clear trend between α_{ME} values and applied frequency. We also notice that self-biased systems tend to have lower α_{ME} values and higher operating frequencies than devices with tip masses and externally biased ME WPT systems.

Figure 18 shows a nearly linear relationship between power density and applied frequency, especially below about 20 kHz. If we imagine a line across the highest performing devices such as Lee *et al* [35], Kambale *et al* [69], Dong *et al* [26], Bian

Table 4. ME WPT, no tip mass, with external bias.

Author	Year/reference	α_{ME} V cm^{-1} Oe^{-1}	Power density mW cm^{-3} Oe^{-2}	Frequency Hz	FOM$_p$ mW cm^{-3} Oe^{-2} Hz^{-1}
Dong	2008/[26]	2250	2.1	2100	1×10^{-3}
O'Handley	2008/[1]	25.2	4.9	60 000	8.2×10^{-5}
Bian	2009/[49]	375.875	5.4	26 600	2×10^{-4}
Li	2010/[38]	25	3.1	27 000	1.1×10^{-6}
Wang	2010/[50]	60	7.4	83 600	8.9×10^{-5}
Onuta	2011/[57]	33.6	6.9×10^{-1}	3800	1.8×10^{-4}
Rizzo	2019/[52]	5.2	7.7×10^{-1}	200 000	3.8×10^{-6}
Malleron	2019/[55]	243	1.6	70 000	2.3×10^{-5}
Truong	2020/[8]	40.8	2.7	70 470	3.9×10^{-5}
Reis	2016/[58]	250	5.6	54 500	1×10^{-4}
Li	2010/[66]	137.5	4.1	64 000	6.4×10^{-5}
Lasheras	2015/[59]	145.6	7.3	46 800	1.5×10^{-4}
Singer	2020/[63]	—	1.2	400 000	3.1×10^{-6}
Newacheck	2020/[65]	—	7.9×10^{-2}	43 000	1.8×10^{-6}

Table 5. ME WPT, self-biased.

Author	Year/reference	α_{ME} V cm^{-1} Oe^{-1}	Power density, mW cm^{-3} Oe^{-2}	Frequency Hz	FOM$_p$ mW cm^{-3} Oe^{-2} Hz^{-1}
Ma	2016/[72]	15.5	—	1464 000	—
Ma	2016/[74]	29	—	120 000	—
Mandal	2011/[56]	46	—	170	—
Li	2013/[78]	380	—	33 700	—
Chen	2014/[79]	126.625	—	154 520	—
Xu	2015/[80]	19.6	—	115 140	—
Zhang	2014/[81]	13.75	—	97 500	—
Zhang	2013/[22]	39.5	—	119 750	—
Saha	2021/[82]	53.84	3.2	187 600	1.7×10^{-5}
Lage	2012/[86]	96.7	—	1197	—
Zhang	2014/[75]	28	1.5×10^{-3}	111 500	1.4×10^{-8}

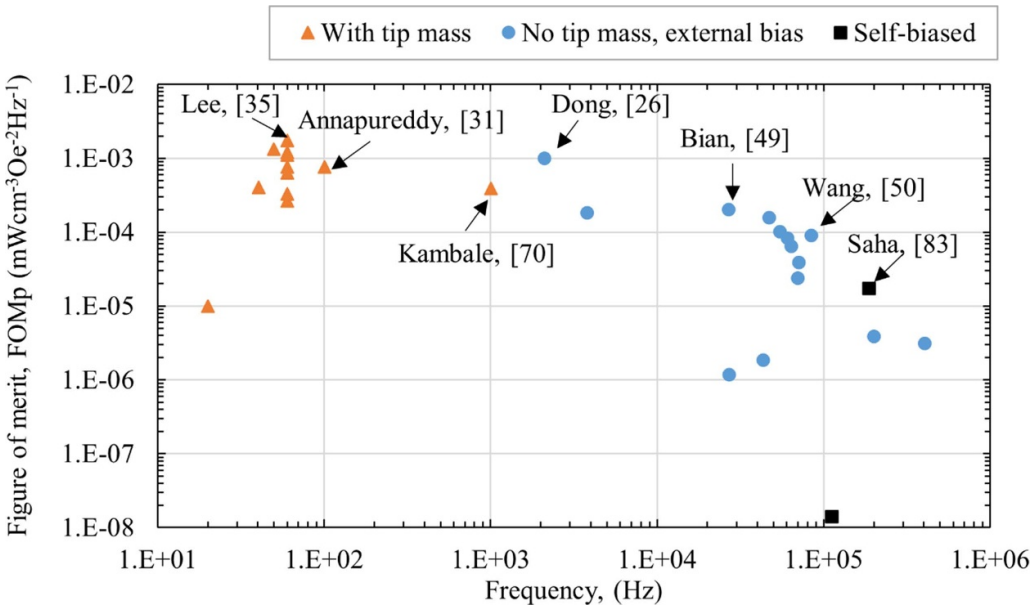

Figure 19. Relationship between power figure of merit and operating frequency.

et al [49], and Wang *et al* [50], we notice power density values have a proportional relationship with operating frequency. According to Truong [88] output power scales linearly with operating frequency, which is supported by the data in this figure. The best reported power density, 7.4 mW cm^{-3} Oe^{-2} for Wang *et al* [50], is a longitudinal mode ME WPT system with external bias.

Figure 19 plots FOM_p vs frequency. For devices operating below 10 kHz, FOM_p is approximately constant with frequency, which is what would be predicted by the theory in [88]. For devices operating at higher frequencies, a negative relationship with frequency does seem evident which would not be predicted by [88]. See section 7 for a further discussion of this point. We can also see that ME WPT systems with tip magnetic masses tend to have higher FOM_p values than the systems without tip masses. Therefore, according to our comparative analysis the most efficient systems are ME WPT systems with magnetic tip masses. We hypothesize that the extra torque added by the tip mass could explain the higher power figures of merit. The best FOM_p, 0.1 mW cm^{-3} Oe^{-2} Hz^{-1} can be observed in this figure by Lee *et al* [35].

7. Discussion and conclusions

Our discussion focuses mostly on ME structures used as receivers in WPT systems. Although ME structures can be used as transmitters as well, this configuration seems to be less common in the literature. The most common configuration is to use a traditional coil as a transmitter and a ME structure as a receiver. This may be due to the fact that such a configuration is more convenient for research studies: it is easier to create a uniform magnetic field with a coil which enables isolated study of the ME structure as a receiver. However, it is also the case that the coil transmitter/ME laminate receiver configuration is practical for many real-world applications. The advantage of ME laminate receivers is their more favorable size-to-frequency relationship. And many attractive applications, such as biomedical implants, require a small receiver but not necessarily a small transmitter. Therefore, this review has spent more effort on both ME structures as receivers in WPT systems and on performance metrics that are applicable to receivers.

Although single phase ME materials have been extensively studied, virtually all of the high performing devices in the scholarly literature are composites of MS and piezoelectric materials. Composites in all the standard configurations (0–3, 1–3, 2–2) have been demonstrated, but the highest performing composites have generally been 2–2 composites or structures that use 2–2 composites (or laminates) as part of the structure. The prevalence of 2–2 composites as ME WPT receivers is likely due to the better stress transfer (i.e. more uniform stress transfer across a larger contacting surface) between MS and piezoelectric layers and their relative ease of manufacture. Given that somewhat narrowed scope, this section discusses some of the overall trends and insights that we see from a review of the relevant literature.

Assuming a 2–2 composite structure, the key material parameters for ME WPT structures for piezoelectric and MS materials are $d_{31,p}/s^{E}_{11}$ and $d_{33,m}/s^{H}_{33}$ respectively. (See section 2 Materials for a more detailed discussion of these material parameters.) The most common piezoelectric materials used in ME laminates are formulations of PZT. In particular 'soft' PZT materials, such as PZT–5H (i.e. Navy Type VI) have a higher piezoelectric figure of merit for ME WPT. Single crystal piezoelectric materials such as PMT–PT are also used as they have a very high $d_{31,p}$ coefficient. However, they are also more compliant and their piezoelectric figure of merit for ME WPT is similar to much less expensive and more readily available soft PZT materials. Another consideration is that soft PZT materials typically have a lower quality factor than hard PZT materials (i.e. PZT–4A) which could hurt performance at resonance. However, in our experience, the limiting factors of the system quality factor are usually anchor loss and adhesives, not the inherent material losses. For a more complete description of the piezoelectric figure of merit and the traditional piezoelectric energy harvesting (or resonator) figure of merit ($d^2_{31,p}/s^2_{11}\varepsilon$) we refer the reader to [8]. As shown in table 1, Metglas (FeSiB) has by far the highest MS figure of merit among common MS materials. Terfenol-D ($Tb_xDy_{1-x}Fe_2$) and Galfenol (FeGa) also have relatively high MS figures of merit. Not surprisingly, the vast majority of ME receiver devices use one of these three materials. Although Metglas has a higher MS figure of merit, Terfenol-D and Galfenol have a much higher saturation magnetostriction which can be useful in some applications. Secondly, Metglas is typically supplied only in thin ribbons (approximately 25 μm in thickness). Although these thin ribbons can be laminated together, if a much thicker MS layer is needed, Terfenol-D or Galfenol may be better approaches.

To compare different devices and types of structures we have chosen a power figure of merit (FOM_p) that normalizes for device volume, applied AC magnetic field squared, and frequency. As we have described, and as has been reported in many published works, power output scales with device volume and with the square of the applied magnetic field. For this reason we believe that FOM_p is a better figure of merit for ME WPTS than the ME coefficient (α_{ME}), which normalizes for piezoelectric layer thickness and magnetic field to the first power. (α_{ME} is clearly more relevant for sensing applications in which the output voltage magnitude is the critical parameter). Figure 15 also suggests that among published ME WPT receivers there is no obvious relationship between α_{ME} and power density. The appropriate relationship between an applicable figure of merit and frequency is less obvious from the literature. Based on the analysis of Truong [88], power for ME WPT receivers should scale linearly with frequency assuming that the mechanical quality factor is constant with frequency. Given this analysis, and the fact the FOM_p normalizes for frequency, we would expect that FOM_p would be approximately constant with frequency, and indeed this does seem to be true below about 10 kHz (see figure 18). However, at higher frequencies FOM_p seems to fall with increasing frequency. This same effect can be seen in figure 17 in which

power density stops increasing with frequency for devices at higher frequencies. It is not immediately clear why the trend with frequency changes for the higher frequency devices. One hypothesis is that the mechanical quality factor is indeed constant with frequency for the lower frequency devices, but for the higher frequency devices, which are mostly longitudinal mode resonators, the quality factor decreases with frequency. Further analysis would be needed to explore this hypothesis. A second possible hypothesis is that the decreasing performance with frequency is due to different relative contributions from the MS and piezoelectric materials. If, for example, higher frequency devices have different MS materials or less MS material relative to the amount of piezoelectric material, the power figure of merit could suffer. A third possible hypothesis is the power loss due to the effects of the demagnetizing field, a critical factor for MS materials with high permeability. The influence of the demagnetization phenomenon on the maximum output power was briefly discussed in [88]. FOM_p does not account for these effects. However, we are still confident that FOM_p represents the most relevant figure of merit of those proposed for ME WPT receivers.

We have categorized ME laminate receiver structures into three broad categories: ME–MME, ME longitudinal mode, and ME bending mode. See section 3 Device Approaches for examples of all three types of structures. ME–MME structures very slightly outperform ME longitudinal mode structures on average when considering the power figure of merit. Although it should be noted that the ME–MME structures operate at much lower frequencies, and thus tend to have lower power densities even though they have a slightly higher power figures of merit. ME–MME structures contain a permanent magnet that augments the ME laminate. The permanent magnet can have two effects: first, the torque resulting from the interaction between the magnet and external magnetic field combines with the force from the MS material to amplify the magnitude of the ME structure vibrations which may account for their slightly higher power figure of merit, and second, the mass from the magnet reduces the resonance frequency which is useful for low frequency applications. As the name implies, ME longitudinal mode devices do not operate in bending mode and have no permanent magnet. For higher frequency devices (i.e. 1 kHz–1 MHz) rectangular ME laminates operating in longitudinal mode are the most common type of structure. There are a few examples of more complex structures that make use of 2–2 ME composites operating in longitudinal extension mode [38, 66], although they do not seem to outperform the standard rectangular laminates according to the power figure of merit. Perhaps the reason that the simple rectangular laminate is most common is simply ease of manufacture. Truong and Roundy [8] have shown that in most cases, maximizing the performance of a ME laminate relies more heavily on increasing the performance (i.e. piezomagnetic constant or amount of material) of the MS phase than the piezoelectric phase. So, it stands to reason that adding a permanent magnet, which also increases the magnetic-to-mechanical coupling, or a rectangular laminate as opposed to a more complex structure with less MS material per overall volume would result in a higher power figure of merit. This logical conclusion is consistent with a comparison of published devices as shown in tables 3 and 4.

Referring to figure 12, the piezomagnetic constant $d_{33,m}$ is a function of the applied magnetic field. In order to operate at point where $d_{33,m}$ is highest, either the applied AC magnetic field must be large enough in amplitude such that the peak of the $d_{33,m}$ curve is reached, or a DC bias field with a smaller superimposed AC magnetic field must be applied. Usually the second approach is used as the fields required to reach maximum $d_{33,m}$ are quite large, on the order of 10–100 Oe for Metglas and 100–1000 Oe for Terfenol-D and Galfenol. The DC bias field is usually either applied with an external coil (usually a Helmholtz coil), external magnets placed near, but not on, the ME structure, or magnets placed directly on the MS material. External biasing coils and magnets work well for laboratory experiments, but with few exceptions these approaches are not appropriate for final applications. In many instances, magnets placed directly on the MS material may be appropriate in an end application. However, for some applications, such as biomedical implants, permanent magnets can cause safety and/or reliability concerns. All three methods are capable of applying the optimal DC bias. Given that the permanent magnets are problematic for many applications, there has been significant research on methods to self-bias ME composite structures (see section 5). Performance metrics for devices employing these various methods are summarized in table 5. Most self-biased devices in the literature report the ME voltage coefficient, α_{ME}, but do not give enough information to calculate FOM_P. Self-biased devices perform similarly to externally biased in terms of α_{ME}. The two devices for which data does allow the calculation of FOM_P [75, 82], report values of 1.4×10^{-8} and are 1.7×10^{-5} mW Oe^{-2} cm^{-3} Hz^{-1}. The second of these is similar to externally biased devices operating at similar frequencies. Thus, although there is still much work to be done on self-biased devices, those reported in the literature are within the performance range of externally biased devices. The best performing self-biased devices use the magnetization grading approach. However, as self-biasing methods are an area of active research, it would be premature to conclude that the magnetization grading is the preferred approach, but it does seem promising.

The past several years have seen an increasing amount of research on ME devices used in WPT applications. With few exceptions, ME WPTS receivers are rectangular laminates of MS and piezoelectric materials, sometimes with a magnet proof mass attached. There has been relatively little work on geometry optimization combined with fabrication methods that might make more creative geometries possible. We have reviewed recent research on self-biasing techniques, however, this is an active area of research with much more to be learned and a significant next step in ME WPTS research. Several approaches have been demonstrated, but issues remain. For example, one approach, annealing Metglas under a magnetic field results in very fragile material that lacks robustness. Sufficient data on the longevity of devices that utilize pre-magnetized MS material is lacking. Other methods, such as

exchange biasing, require complicated and expensive fabrication methods. We believe research to improve the performance of self-biased devices and address these issues is highly warranted. Finally, we are unaware of studies investigating the safety of ME devices for biomedical implants especially considering such issues as magnetic resonance imaging (MRI) compatibility. In our opinion, all of these areas merit further research.

Data availability statement

All data that support the findings of this study are included within the article (and any supplementary files).

Acknowledgment

This material is based upon work supported by the National Science Foundation under Grant No. 1651438.

ORCID iDs

Orpita Saha https://orcid.org/0000-0002-1733-8804
Binh Duc Truong https://orcid.org/0000-0001-7108-4713
Shad Roundy https://orcid.org/0000-0002-5256-628X

References

[1] O'Handley R C, Huang J K, Bono D C and Simon J 2008 Improved wireless, transcutaneous power transmission for *in vivo* applications *IEEE Sens. J.* **8** 57–62
[2] Basaeri H, Christensen D B and Roundy S 2016 A review of acoustic power transfer for bio-medical implants *Smart Mater. Struct.* **25** 123001
[3] Kim S, Ho J S, Chen L Y and Poon A S Y 2012 Wireless power transfer to a cardiac implant *Appl. Phys. Lett.* **101** 073701
[4] Ho J S, Yeh A J, Neofytou E, Kim S, Tanabe Y, Patlolla B, Beygui R E and Poon A S Y 2014 Wireless power transfer to deep-tissue microimplants *Proc. Natl Acad. Sci. USA* **111** 201403002
[5] Lin J C 2006 Radio-frequency radiation safety and health *Radio Sci. Bull.* **317** 107–8
[6] Ziegelberger G *et al* 2020 International commission on non-ionizing radiation protection (ICNIRP), guidelines for limiting exposure to electromagnetic fields (100 kHz to 300 GHz) *Health Phys.* **118** 483–524
[7] Awal M R, Jusoh M, Sabapathy T, Kamarudin M R and Rahim R A 2016 State-of-the-art developments of acoustic energy transfer *Int. J. Antennas Propag.* **2016** 1–14
[8] Truong B D and Roundy S 2020 Experimentally validated model and power optimization of a magnetoelectric wireless power transfer system in free-free configuration *Smart Mater. Struct.* **29** 085053
[9] Truong B D, Andersen E, Casados C and Roundy S 2020 Magnetoelectric wireless power transfer for biomedical implants: effects of non-uniform magnetic field, alignment and orientation *Sens. Actuators* A **316** 112269
[10] Palneedi H, Annapureddy V, Priya S and Ryu J 2016 Status and perspectives of multiferroic magnetoelectric composite materials and applications *Actuators* **5** 9
[11] Eerenstein W, Mathur N D and Scott J F 2006 Multiferroic and magnetoelectric materials *Nature* **442** 759–65
[12] Jiles D 2016 *Introduction to Magnetism and Magnetic Materials* 3rd edn (Boca Raton, FL: CRC Press)
[13] Engdahl G and Mayergoyz I D 2000 *Handbook of Giant Magnetostrictive Materials* (San Diego: Academic)
[14] Wang Y, Hu J, Lin Y and Nan C W 2010 Multiferroic magnetoelectric composite nanostructures *NPG Asia Mater.* **2** 61–68
[15] Nan C-W 1994 Magnetoelectric effect in composites of piezoelectric and piezomagnetic phases *Phys. Rev.* B **50** 6082–8
[16] Chu Z, Pourhosseiniasl M and Dong S 2018 Review of multi-layered magnetoelectric composite materials and devices applications *J. Phys. D: Appl. Phys.* **51** 243001
[17] Ryu J, Carazo A V, Uchino K and Kim H E 2001 Magnetoelectric properties in piezoelectric and magnetostrictive laminate composites *Jpn. J. Appl. Phys.* **40** 4948
[18] Ma J, Hu J, Li Z and Nan C W 2011 Recent progress in multiferroic magnetoelectric composites: from bulk to thin films *Adv. Mater.* **23** 1062–87
[19] Annapureddy V, Palneedi H, Hwang G-T, Peddigari M, Jeong D-Y, Yoon W-H, Kim K-H and Ryu J 2017 Magnetic energy harvesting with magnetoelectrics: an emerging technology for self-powered autonomous systems *Sustain. Energy Fuels* **1** 2039–52
[20] Dong S, Li J F and Viehland D 2004 Characterization of magnetoelectric laminate composites operated in longitudinal-transverse and transverse-transverse modes *J. Appl. Phys.* **95** 2625–30
[21] Hockel J L, Wu T and Carman G P 2011 Voltage bias influence on the converse magnetoelectric effect of PZT/terfenol-D/PZT laminates *J. Appl. Phys.* **109** 064106
[22] Zhang J, Li P, Wen Y, He W, Yang A and Lu C 2013 Giant self-biased magnetoelectric response with obvious hysteresis in layered homogeneous composites of negative magnetostrictive material Samfenol and piezoelectric ceramics *Appl. Phys. Lett.* **103** 202902
[23] Dong S, Li J F and Viehland D 2003 Giant magneto-electric effect in laminate composites *IEEE Trans. Ultrason. Ferroelectr. Freq. Control* **50** 1236–9
[24] Piezo Acoustics 2020 *PVdF Film - Its Properties and Uses* (Piezo Acoustics Ltd)
[25] Truong B D, Williams S and Roundy S 2019 Experimentally validated model and analytical investigations on power optimization for piezoelectric-based wireless power transfer systems *J. Intell. Mater. Syst. Struct.* **30** 2464–77
[26] Dong S, Zhai J, Li J F, Viehland D and Priya S 2008 Multimodal system for harvesting magnetic and mechanical energy *Appl. Phys. Lett.* **93** 103511
[27] Gao J, Hasanyan D, Shen Y, Wang Y, Li J and Viehland D 2012 Giant resonant magnetoelectric effect in bi-layered Metglas/Pb (Zr, Ti) O_3 composites *J. Phys. D: Appl. Phys.* **112** 104101
[28] Ryu J *et al* 2015 Ubiquitous magneto-mechano-electric generator *Energy Environ. Sci.* **8** 2402–8
[29] Annapureddy V *et al* 2016 Low-loss piezoelectric single-crystal fibers for enhanced magnetic energy harvesting with magnetoelectric composite *Adv. Energy Mater.* **6** 1–10
[30] Annapureddy V *et al* 2016 Enhanced magnetic energy harvesting properties of magneto-mechano-electric generator by tailored geometry *Appl. Phys. Lett.* **109** 093901
[31] Annapureddy V *et al* 2018 Exceeding milli-watt powering magneto-mechano-electric generator for standalone-powered electronics *Energy Environ. Sci.* **11** 818–29
[32] Kang M G, Sriramdas R, Lee H, Chun J, Maurya D, Hwang G T, Ryu J and Priya S 2018 High power magnetic

field energy harvesting through amplified magneto-mechanical vibration *Adv. Energy Mater.* **8** 1–11
[33] Lu Y, Chen J, Cheng Z and Zhang S 2019 The PZT/Ni unimorph magnetoelectric energy harvester for wireless sensing applications *Energy Convers. Manage.* **200** 112084
[34] Sriramdas R, Kang M-G, Meng M, Kiani M, Ryu J, Sanghadasa M and Priya S 2020 Large power amplification in magneto-mechano-electric harvesters through distributed forcing *Adv. Energy Mater.* **10** 1903689
[35] Lee H, Sriramdas R, Kumar P, Sanghadasa M, Kang M G and Priya S 2020 Maximizing power generation from ambient stray magnetic fields around smart infrastructures enabling self-powered wireless devices *Energy Environ. Sci.* **13** 1462–72
[36] Song H, Patil D R, Yoon W-H, Kim K-H, Choi C, Kim J-H, Hwang G-T, Jeong D-Y and Ryu J 2020 Significant power enhancement of magneto-mechano-electric generators by magnetic flux concentration *Energy Environ. Sci.* **13** 4238–48
[37] Rupp T, Truong B D, Williams S and Roundy S 2019 Magnetoelectric transducer designs for use as wireless power receivers in wearable and implantable applications *Materials* **12** 512
[38] Li P, Wen Y, Liu P, Li X and Jia C 2010 A magnetoelectric energy harvester and management circuit for wireless sensor network *Sens. Actuators* A **157** 100–6
[39] Li P, Wen Y and Bian L 2007 Enhanced magnetoelectric effects in composite of piezoelectric ceramics, rare-earth iron alloys, and ultrasonic horn *Appl. Phys. Lett.* **90** 022503
[40] Lal A and White R M 1996 Silicon microfabricated horns for power ultrasonics *Sens. Actuators* A **54** 542–6
[41] Bayrashev A, Robbins W P and Ziaie B 2004 Low frequency wireless powering of microsystems using piezoelectric-magnetostrictive laminate composites *Sens. Actuators* A **114** 244–9
[42] Chlaihawi A A, Emamian S, Narakathu B B, Bazuin B J and Atashbar M Z 2017 Novel screen printed and flexible low frequency magneto-electric energy harvester *2016 IEEE Sensors* 13–15
[43] Guo M and Dong S 2009 A resonance-bending mode magnetoelectric-coupling equivalent circuit *IEEE Trans. Ultrason. Ferroelectr. Freq. Control* **56** 2578–86
[44] Guo L, Zhang H, Lu R and Yu G 2015 Magnetoelectric analysis of a bilayer piezoelectric/magnetostrictive composite system with interfacial effect *Compos. Struct.* **134** 285–93
[45] Li L, Chen X M and Zhu H Y 2013 Unique dependence of magnetoelectric voltage coefficient on bias magnetic field in Terfenol-D/Pb(Zr,Ti)O_3 bi-layered composites *J. Alloys Compd.* **553** 86–88
[46] Sudersan S, Maniprakash S and Arockiarajan A 2018 Nonlinear magnetoelectric effect in unsymmetric laminated composites *Smart Mater. Struct.* **27** 125005
[47] Lafont T, Gimeno L, Delamare J, Lebedev G A, Zakharov D I, Viala B, Cugat O, Galopin N, Garbuio L and Geoffroy O 2012 Magnetostrictive-piezoelectric composite structures for energy harvesting *J. Micromech. Microeng.* **22** 094009
[48] Olabi A G and Grunwald A 2008 Design and application of magnetostrictive materials *Mater. Des.* **29** 469–83
[49] Bian L, Wen Y, Li P, Gao Q and Zheng M 2009 Magnetoelectric transducer with high quality factor for wireless power receiving *Sens. Actuators* A **150** 207–11
[50] Wang Y, Zhao X, Jiao J, Liu L, Di W, Luo H and Or S W 2010 Electrical resistance load effect on magnetoelectric coupling of magnetostrictive/piezoelectric laminated composite *J. Alloys Compd.* **500** 224–6
[51] Wang Y, Or S W, Chan H L W, Zhao X and Luo H 2008 Enhanced magnetoelectric effect in longitudinal-transverse mode Terfenol-D/Pb ($Mg_1/_3Nb_2/_3$) O_3-$PbTiO_3$ laminate composites with optimal crystal cut *J. Appl. Phys.* **103** 124511
[52] Rizzo G, Loyau V, Nocua R, Lourme J C and Lefeuvre E 2019 Potentiality of magnetoelectric composites for wireless power transmission in medical implants *Int. Symp. Medical Information and Communication Technology (ISMICT)* vol 2019 pp 2019–22
[53] Ahlbom A *et al* 1998 Guidelines for limiting exposure to time-varying electric, magnetic, and electromagnetic fields (UP TO 300 GHz) *Health Phys.* **74** 494–522
[54] Bailey W H *et al* 2019 Synopsis of IEEE Std C95.1™-2019 'IEEE standard for safety levels with respect to human exposure to electric, magnetic, and electromagnetic fields, 0 Hz to 300 GHz' *IEEE Access* **7** 171346–56
[55] Malleron K, Gensbittel A, Talleb H and Ren Z 2019 Experimental study of magnetoelectric transducers for power supply of small biomedical devices *Microelectron. J.* **88** 184–9
[56] Mandal S K, Sreenivasulu G, Petrov V M and Srinivasan G 2011 Magnetization-graded multiferroic composite and magnetoelectric effects at zero bias *Phys. Rev.* B **84** 1–8
[57] Onuta T D, Wang Y, Long C J and Takeuchi I 2011 Energy harvesting properties of all-thin-film multiferroic cantilevers *Appl. Phys. Lett.* **99** 2009–12
[58] Reis S, Silva M P, Castro N, Correia V, Rocha J G, Martins P, Lasheras A, Gutierrez J and Lanceros-Mendez S 2016 Electronic optimization for an energy harvesting system based on magnetoelectric Metglas/poly(vinylidene fluoride)/Metglas composites *Smart Mater. Struct.* **25** 085028
[59] Lasheras A, Gutiérrez J, Reis S, Sousa D, Silva M, Martins P, Lanceros-Mendez S, Barandiarán J M, Shishkin D A and Potapov A P 2015 Energy harvesting device based on a metallic glass/PVDF magnetoelectric laminated composite *Smart Mater. Struct.* **24** 065024
[60] Zaeimbashi M *et al* 2021 Ultra-compact dual-band smart NEMS magnetoelectric antennas for simultaneous wireless energy harvesting and magnetic field sensing *Nat. Commun.* **12** 31–41
[61] Yu Z *et al* 2020 ISSCC 2020/session 34/biomedical sensing, stimulation & harvesting/34. 3 *2020 IEEE Int. Solid- State Circuits Conf.* pp 292–4
[62] Khalifa A *et al* 2021 Magnetoelectric versus inductive power delivery for sub-mm receivers *2021 IEEE MTT-S Wireless Power Transfer Conf. (WPTC 2021)* 1–4
[63] Singer A *et al* 2020 Magnetoelectric materials for miniature, wireless neural stimulation at therapeutic frequencies *Neuron* **107** 631–43
[64] Park S H, Kumar A, Kaarthik J, Annapureddy V and Ryu J 2020 A magneto-mechano-electric generator based on lead-free single-crystal fibers for robust scavenging of ambient magnetic energy *Electron. Mater. Lett.* **16** 369–75
[65] Newacheck S and Youssef G 2020 Wireless energy transfer based on strain-mediated composite multiferroics *Smart Mater. Struct.* **29** 015014
[66] Li P, Wen Y M, Jia C B and Li X S 2011 A magnetoelectric composite energy harvester and power management circuit *IEEE Trans. Ind. Electron.* **58** 2944–51
[67] Zhou Y, Maurya D, Yan Y, Srinivasan G, Quandt E and Priya S 2016 Self-biased magnetoelectric composites: an overview and future perspectives *Energy Harvest. Syst.* **3** 1–42
[68] Patil D R, Zhou Y, Kang J-E, Sharpes N, Jeong D-Y, Kim Y-D, Kim K H, Priya S and Ryu J 2014 Anisotropic self-biased dual-phase low frequency magneto-mechano-electric energy harvesters with giant power densities *APL Mater.* **2** 046102

[69] Kambale R C *et al* 2014 Magneto-mechano-electric (MME) energy harvesting properties of piezoelectric macro-fiber composite/Ni magnetoelectric generator *Energy Harvest. Syst.* **1** 3-11

[70] Kulkarni A, Meurisch K, Teliban I, Jahns R, Strunskus T, Piorra A, Knöchel R and Faupel F 2014 Giant magnetoelectric effect at low frequencies in polymer-based thin film composites *Appl. Phys. Lett.* **104** 022904

[71] Jin J, Lu S G, Chanthad C, Zhang Q, Haque M A and Wang Q 2011 Multiferroic polymer composites with greatly enhanced magnetoelectric effect under a low magnetic bias *Adv. Mater.* **23** 3853–8

[72] Ma J, Xin C, Ma J, Zhang Q and Nan C 2016 Self-biased magnetoelectric effect in (Pb, Zr)TiO_3/metglas laminates by annealing method *Sci. Bull.* **61** 378–82

[73] Cadogan J M, Campbell S J, Jing J, Foley C P, Kater P and Mai Y W 2014 Annealing embrittlement of $Fe_{78}Si_9B_{13}$ (METGLAS-2605S2) *Hyperfine Interact.* **226** 7–14

[74] Ma J N, Xin C Z, Ma J, Lin Y H and Nan C W 2016 A cost-effective self-biased magnetoelectric effect in $SrFe_{12}O_{19}$/Metglas/Pb(Zr,Ti)O_3 laminates *J. Phys. D: Appl. Phys.* **49** 405002

[75] Zhang J, Li P, Wen Y, He W, Yang A and Lu C 2014 Shear-mode self-biased magnetostrictive/piezoelectric laminate multiferroic heterostructures for magnetic field detecting and energy harvesting *Sens. Actuators* A **214** 149–55

[76] Mantese J V, Micheli A L, Schubring N W, Hayes R W, Srinivasan G and Alpay S P 2005 Magnetization-graded ferromagnets: the magnetic analogs of semiconductor junction elements *Appl. Phys. Lett.* **87** 1–4

[77] Sudakar C, Naik R, Lawes G, Mantese J V, Micheli A L, Srinivasan G and Alpay S P 2007 Internal magnetostatic potentials of magnetization-graded ferromagnetic materials *Appl. Phys. Lett.* **90** 4–7

[78] Li M, Wang Z, Wang Y, Li J and Viehland D 2013 Giant magnetoelectric effect in self-biased laminates under zero magnetic field *Appl. Phys. Lett.* **102** 8–11

[79] Chen L, Li P, Wen Y and Zhu Y 2014 Large self-biased effect and dual-peak magnetoelectric effect in different three-phase magnetostrictive/piezoelectric composites *J. Alloys Compd.* **606** 15–20

[80] Xu X, Qiu J, Wen Y, Li P, Chen H and Liu X 2015 Zero-biased magnetoelectric effects in five-phase laminate composites with FeCoV soft magnetic alloy *IEEE Trans. Magn.* **51** 1–4

[81] Zhang J *et al* 2014 High-sensitivity laminated magnetoelectric sensors without bias in composite of positive/negative giant magnetostrictive materials and piezoelectric single crystals *J. Appl. Phys.* **115** 17E517

[82] Saha O, Andersen E and Roundy S 2021 Wireless power transfer by self-biased magnetoelectric laminate for biomedical implants *2021 IEEE 20th Int. Conf. Micro and Nanotechnology for Power Generation and Energy Conversion Applications MEMS 2021* pp 36–39

[83] Stamps R L 2000 Mechanisms for exchange bias *J. Phys. D: Appl. Phys.* **33** R247–68

[84] Nogués J and Schuller I K 1999 Exchange bias *J. Magn. Magn. Mater.* **192** 203–32

[85] Berkowitz A E and Takano K 1999 Exchange anisotropy—a review *J. Magn. Magn. Mater.* **200** 552–70

[86] Lage E, Kirchhof C, Hrkac V, Kienle L, Jahns R, Knöchel R, Quandt E and Meyners D 2012 Biasing of magnetoelectric composites *Nat. Mater.* **11** 523–9

[87] Lage E, Urs N O, Röbisch V, Teliban I, Knöchel R, Meyners D, McCord J and Quandt E 2014 Magnetic domain control and voltage response of exchange biased magnetoelectric composites *Appl. Phys. Lett.* **104** 132405

[88] Truong B D 2021 Power optimization of a magnetoelectric wireless power transfer system with volume constraint *Sens. Actuators* A **341** 113226